RESEARCH REPORT

RADIATION EFFECTS ON LIQUID PROPELLANTS

to

NATIONAL AERONAUTICS AND SPACE ADMINISTRATION

February 2, 1970

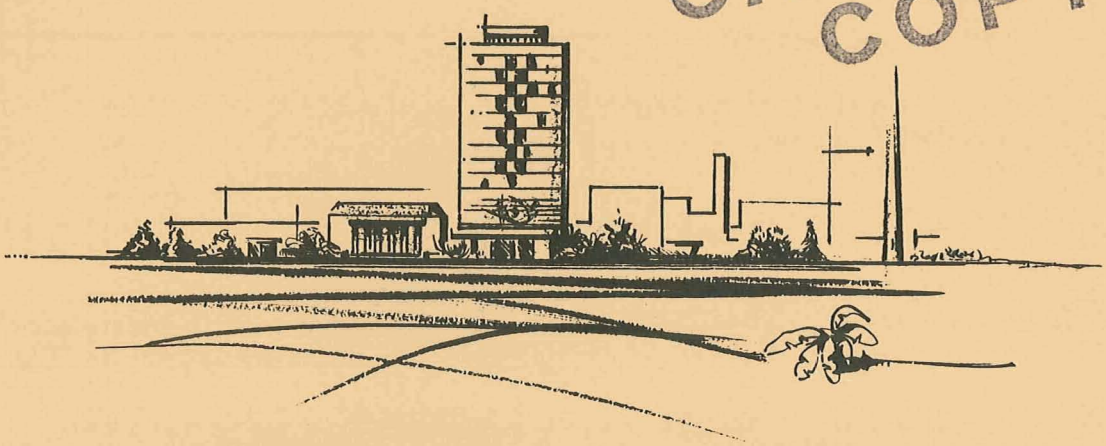

BATTELLE MEMORIAL INSTITUTE

COLUMBUS LABORATORIES

THE COLUMBUS LABORATORIES of Battelle Memorial Institute comprise the original research center of an international organization devoted to research.

The Institute is frequently described as a "bridge" between science and industry – a role it has performed in more than 90 countries. As an independent research institute, it conducts research encompassing virtually all facets of science and its application. It also undertakes programs in fundamental research and education.

Battelle-Columbus – with its staff of 3,000 – serves industry and government through contract research. It pursues:

- research embracing the physical and life sciences, engineering, and selected social sciences
- design and development of materials, products, processes, and systems
- information analysis, socioeconomic and technical economic studies, and management planning research.

505 KING AVENUE • COLUMBUS, OHIO 43201

CR 109767

FINAL REPORT

on

RADIATION EFFECTS ON LIQUID PROPELLANTS

to

NATIONAL AERONAUTICS AND SPACE ADMINISTRATION

February 2, 1970

by

J. F. Kircher, R. E. Best, and J. E. Rollins

Prepared For
The Jet Propulsion Laboratory
Pasadena, California 91103

Under National Aeronautical and Space
Administration Contract NAS7-722

BATTELLE MEMORIAL INSTITUTE
Columbus Laboratories
505 King Avenue
Columbus, Ohio 43201

TABLE OF CONTENTS

TABLE OF CONTENTS (Continued)

ABSTRACT

The effects of ionizing radiation on selected liquid propellants have been investigated and preliminary development of a comprehensive computer program for shield optimization has been completed. Gamma-ray attenuation parameters for six candidate propellant materials have been calculated. These data are formulated into linear attenuation coefficients and buildup factors which are tabulated. A logic flow diagram for generalized weight optimization to select shield configurations for various propellant materials was generated and a simplified computer program which minimizes the weight of a primary direct laminated shield was developed. Radiation effects on three fuels and three oxidizers were investigated in several container materials and over a range of dose rates. Propellant materials investigated include: FLOX, oxygen difluoride, nitrogen tetroxide (inhibited and uninhibited), diborane, hydrazine, and the LPG fuel, propane. In general, it was found that oxidizers are much less susceptible to radiation induced decomposition than fuels and differences due to dose rate are generally not large.

RADIATION EFFECTS ON LIQUID PROPELLANTS

INTRODUCTION

It is advantageous to use high specific impulse liquid propellants on long-term space probes using isotope or nuclear power sources for auxiliary power because of the rigid weight and volume requirements on such missions. However, more definitive knowledge of environmental effects on the long-term storability of these propellants is desirable so that design engineers may have reasonable assurance that the stored propellant system chosen for a particular mission will fulfill its function successfully. A preliminary study under Contract NAS7-577 was carried out to ascertain the state of the art regarding radiation effects data on liquid propellants and to analyze the suitability of using various propellant systems on space probes with different auxiliary power sources.

The present program was established with the objective of developing more detailed information on radiation effects and shielding requirements for a few selected liquid propellants. Three tasks were established in this program. Task 1 was to obtain radiation effects data on three fuels and three oxidizers irradiated as liquids. Task 2 was to begin development of a computer program to ascertain what special design criteria or shielding techniques must be employed to protect components of the propulsion system from radiation, if necessary. Task 3 was a Phase 1 storage test in a low dose rate radiation field extending over a period of months. Results on all three tasks are detailed in the following sections. Task 2, Radiation Shielding Optimization, is discussed in the first section of the report. Tasks 1 and 3 are then discussed in the following sections. Results from both Tasks 1 and 3 are reported together for a given material so that results may be more easily compared and evaluated. Wherever possible, data have been presented in engineering units to facilitate their use among the widest possible audience. Where units specific to radiation effects studies, such as G-values, have been used, an explanation of the term and its use has been given.

RADIATION SHIELDING OPTIMIZATION

Task 2

In a study previously conducted by Battelle's Columbus Laboratories for the National Aeronautics and Space Administration (NAS7-577), the probable types, spectra, and intensities of radiation from nuclear power sources which may possibly be used in deep space missions were determined. The approach followed in the study was a conservative one, i.e., that of determining radiation intensities on the basis of an extrapolated point source without consideration of the self-shielding inherent in a nuclear power source of finite geometry. The results of the study indicated that radiation damage to liquid propellants from certain types of isotopic heat sources, viz., $^{238}PuO_2$ and

$^{244}Cm_2O_3$, which are primarily alpha emitters, would most likely* be insignificant even in unshielded cases for source power levels up to 200 kw (thermal) and corresponding mission lifetimes extending to 5 years. Conversely, the same study revealed that in the case of other power sources investigated, e.g., $^{90}SrTiO_3$, ^{60}Co (metal) and low-powered nuclear reactor sources such as the SNAP-10A reactor, radiation damage to liquid propellants could be a significant problem and, therefore, should be further investigated from the standpoint of reducing the radiation environment. It must be remembered, however, that the significance of a given radiation effect is largely determined by the proposed application of the material under investigation. Thus, as described in later sections of this report, the changes in chemical composition resulting from irradiation of the propellant materials investigated were in general very small and probably not significant from the standpoint of their chemical properties. However, in most cases such small chemical changes were accompanied by the accumulation of noncondensible gaseous products of the liquid propellant samples. The continual buildup of pressure over the liquid propellant could present severe engineering problems, particularly on long missions, even though the total liquid decomposed or chemically altered was small.

Attenuation of the radiation intensity in the vicinity of the propellant can be accomplished by (1) the use of a radiation shield and/or (2) an increased separation distance between the nuclear power source and the liquid propellant. However, overall system requirements (i.e., weight and configuration restrictions, etc.) may limit the extent to which either of the foregoing techniques may be utilized; therefore, a method of systems analysis is required which will consider the nuclear power source, shield, and propellant subsystems within the system restraints while insuring that radiation damage to the propellant does not reach some critical level.

The ultimate selection of optimum liquid propellants for deep space missions may well be predicted on the shielding properties of these materials. Consider, for example, the case where a particular propellant is initially chosen on the basis that it requires only a minimum shield in the close proximity of the nuclear power source while receiving an integrated dose below its radiation damage threshold. Further analysis, however, of the overall system restraints may well indicate the necessity to increase the initially determined shield thickness and/or the source-to-propellant separation distance. A restraint of the latter type would be the allowable integrated dose for the transistors in the instrument package (subsystem) which might possibly be exceeded for the shield and geometric configuration determined above. Therefore, an increase in either of the two parameters, viz., shield thickness and source-to-propellant separation distance, in an effort to preclude the possibility of exceeding the dose limitation for transistors will correspondingly reduce the integrated dose encountered by the propellant, and may possibly permit the selection of a liquid propellant which had previously been eliminated on the basis of radiation damage.

---

* Due to a lack of experimental data for the neutron irradiation of liquid propellants, there is some uncertainty concerning the radiation effects resulting from (n, α) reactions.

On the basis of the foregoing considerations, an optimum computer program should contain a library* of neutron and gamma radiation attenuation data whereby it would account for the effects of auxiliary (propellant) shielding in the overall system optimization from the standpoint of shield weight.

The results of the initial study to provide the basis for a comprehensive shielding optimization computer program are detailed in the following sections.

Subtask A. Compilation and/or Calculation of Propellant Attenuation Data

Compilation of Photon and Neutron Cross-Section Data

Ten energy group photon cross-section data were obtained for propellant constituents, viz., H, N, O, F, and C, from published sources and prepared in a format compatible with an in-house transport code, ANISN[1]**, for subsequent use in propellant attenuation calculations. These data covered a photon energy range of 0.01 to 4 Mev and consisted of photoelectric, pair production, and Compton scattering cross sections; the latter were represented by the zeroth through third moments of the total transfer matrix for use in anisotropic scattering calculations.

Calculation of Propellant Gamma Attenuation Data

A check-case calculation was made with the ANISN code to simulate a benchmark experiment for gamma-ray transport through water. Water was selected as a shield material for the first calculation because (1) experimental data are readily available for this material and (2) its elemental composition is similar to that of the liquid propellants under consideration. The input data utilized for the calculation included an S_8 angular quadrature, P_3 order of scattering, and spatial mesh size of 2 cm; output data were found to be within 10 percent of the experimental values reported for linear attenuation coefficient (μ) and buildup factors.

On the basis of the good correlation obtained between calculated and experimental results for water, additional ANISN calculations were made to determine the attenuation of gamma rays from a point source in hydrazine (N_2H_4), FLOX, OF_2, LPG (CH_4), N_2O_4, and diborane (B_2H_6). Linear attenuation coefficients and dose buildup factors for gamma-ray penetrations up to 160 cm in these fuels were compiled for up to seven photon energy groups (Table 1).

---

* Or else a subroutine whereby such data could be calculated.

** References appear on page 21.

TABLE 1. PHOTON ENERGY GROUP STRUCTURE

Group No.	Energy Range, Mev
1	4 → 3
2	3 → 2.5
3	2.5 → 2.0
4	2.0 → 1.5
5	1.5 → 1.0
6	1.0 → 0.75
7	0.75 → 0.5

TABLE 2. N_2O_4 BUILDUP FACTOR AND LINEAR ATTENUATION COEFFICIENT DATA

		Penetration Depth (cm)/Buildup Factor			
μ	Group No.	20	40	80	160
0.054	1	1.2	1.7	2.0	2.5
0.061	2	1.3	1.85	2.25	2.75
0.069	3	1.4	2.0	2.5	3.0
0.077	4	1.45	2.0	2.5	2.7
0.085	5	1.5	1.9	2.3	2.4
0.105	6	2.0	2.7	3.6	4.2
0.114	7	1.9	2.4	2.9	2.9

Subtask B. Formulation of Propellant Attenuation Data

The dose buildup factors computed for four penetration depths (20, 40, 80, and 160 cm) and linear attenuation coefficients computed by ANISN are listed by group in Tables 2 through 7.

Subtask C. Construction of Computer Program Logic Diagram

Basic Logic Diagram

Under this task, the program logic for the radiation shielding optimization code was constructed. The sequential flow of the basic program is shown in Figure 1. Segments of the program include (1) input of problem data, (2) preliminary data editing and manipulation, (3) selection of calculational sequences for weight optimization (i.e., monitor control), (4) coarse (Level 1) optimization of shield, (5) fine (Level 2) optimization of shield, and (6) an output edit. Each of these program segments is described below.

Data Input. Data planned for input to the computer program include source type and configuration, source-to-propellant-to-instrument package geometry, shield type (split, laminated, and scatter) and configuration, materials together with initial locations, propellant and instrument package radiation dose limitations, and program options for the calculational methods, shield positions, and level of optimization data edit.

Data Edit. The data edit segment of the code will set up and store, in the proper format geometry, data for the various dose calculation routines, determine the radiation source strength and spectrum as well as arrange other pertinent data in a format appropriate for outlines used in the shield optimization.

Control Monitor. Under control monitorship, iterations and flow controls will be set up for specific vehicle configurations. This segment of the program includes optimum sequencing of the various routines used in the selection of a minimum-weight shield.

Level 1 Optimization. The Level 1 or coarse optimization routine selects the weight-optimized shield configuration and position(s) through the use of transmission matrix tables for shield calculations. This method requires a minimum of machine (computer) time per calculation; however, the accuracy of the results is limited. Primary use of the Level 1 weight optimization is to provide a starting point for the Level 2 optimization. In addition, the Level 1 optimization calculations can be used for parametric studies of space systems where a high level of accuracy is not required.

TABLE 3. FLOX BUILDUP FACTOR AND LINEAR ATTENUATION COEFFICIENT DATA

		Penetration Depth (cm)/Buildup Factor			
μ	Group No.	20	40	80	160
0.045	1	1.2	1.5	2.0	2.5
0.051	2	1.3	1.7	2.2	2.7
0.057	3	1.4	1.9	2.5	3.0
0.064	4	1.5	1.9	2.5	2.7
0.070	5	1.5	1.9	2.5	2.5
0.086	6	1.8	2.3	2.5	3.0
0.092	7	1.7	2.2	2.5	2.9

TABLE 4. OF_2 BUILDUP FACTOR AND LINEAR ATTENUATION COEFFICIENT DATA

		Penetration Depth (cm)/Buildup Factor			
μ	Group No.	20	40	80	160
0.048	1	1.2	1.6	2.1	2.6
0.054	2	1.3	1.8	2.3	2.8
0.061	3	1.4	1.9	2.5	3.0
0.068	4	1.5	2.0	2.6	2.9
0.075	5	1.5	2.0	2.4	2.5
0.093	6	1.9	2.4	2.9	3.0
0.10	7	1.8	2.3	2.7	2.9

TABLE 5. N_2H_4 BUILDUP FACTOR AND LINEAR ATTENUATION COEFFICIENT DATA

		Penetration Depth (cm)/Buildup Factor			
μ	Group No.	20	40	80	160
0.034	1	1.2	1.6	2.2	2.6
0.038	2	1.2	1.6	2.2	2.6
0.043	3	1.3	1.7	2.3	2.6
0.049	4	1.3	1.8	2.4	2.7
0.055	5	1.4	1.7	2.0	2.3
0.068	6	1.6	2.2	3.0	3.9
0.072	7	1.6	2.0	2.5	2.9

TABLE 6. CH_4 BUILDUP FACTOR AND LINEAR ATTENUATION COEFFICIENT DATA

		Penetration Depth (cm)/Buildup Factor			
μ	Group No.	20	40	80	160
0.019	1	1.1	1.2	1.9	2.5
0.021	2	1.1	1.3	1.9	2.6
0.024	3	1.2	1.3	2.0	2.6
0.027	4	1.2	1.4	2.1	2.7
0.031	5	1.2	1.5	2.1	2.8
0.038	6	1.3	1.5	2.2	3.0
0.041	7	1.4	1.7	2.2	2.7

TABLE 7. B_2H_6 BUILDUP FACTOR AND LINEAR ATTENUATION COEFFICIENT DATA

		Penetration Depth (cm)/Buildup Factor			
μ	Group No.	20	40	80	160
0.007	1	1.0	1.1	1.2	2.2
0.0077	2	1.0	1.1	1.3	2.3
0.0089	3	1.0	1.1	1.3	2.1
0.010	4	1.05	1.15	1.4	2.0
0.0115	5	1.05	1.2	1.3	1.8
0.0140	6	1.1	1.2	1.4	1.9
0.016	7	1.1	1.3	1.5	1.9

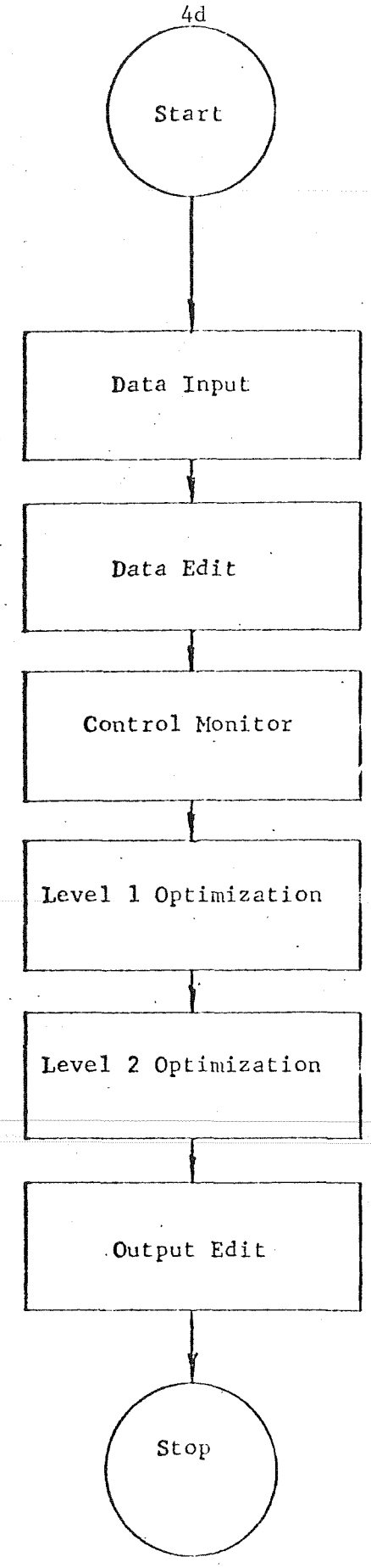

FIGURE 1. BASIC PROGRAM LOGIC DIAGRAM

Level 2 Optimization. The Level 2 optimization routine starts with the Level 1 optimization results and performs a highly accurate weight optimization based on shielding calculations incorporating transport theory. These calculations will evaluate in detail the effects of flux perturbations at shield interfaces, the secondary radiation produced in the shield, propellant and structural members, and the anistropic flux distributions in these members. Both one- and two-dimensional transport-theory calculations will be required to obtain the highly accurate weight-optimized systems.

Output Edit. In the output edit segment of the code, the calculational data generated during the optimization are edited. All data required for the weight optimization are printed.

Semidetailed Logic Diagram

The semidetailed logic for the Level 1 and Level 2 optimization segments of the basic computer program (see previous section) is illustrated in Figures 2, 3, and 4.* The diagram in Figure 2 includes a portion of the logic centered with shield structure (laminations) and position as well as weight optimization of the shield. Figure 3 illustrates the optimization logic for split-shield systems. Figure 4 illustrates the optimization logic for systems recurring scatter-shield analyses. Details of the optimization routine have been omitted in order to illustrate the basic logic of these segments of the program.

Analytical Model on Which Program Logic is Based

The analytical model illustrated in Figure 5 with spherical oxidizer and fuel tanks in tandem has served as the generalized framework for the computer program logic under construction. It is assumed that the component (oxidizer or fuel) having the higher resistance to radiation damage will be located between the remaining component and the radiation source.

Subtask D. Preliminary Programming of Selected Operations of Computer Model

The optimization of the "primary direct laminated shield" was chosen as the selected operation of the computer model to be programmed in this contract performance period (see enclosed portion of logic diagram in Figure 6). The program is written for use in both the Level 1 and Level 2 optimization segments of the generalized computer program (see Figure 1) which is to be developed in the future. The difference between Level 1 and Level 2 uses of this routine will be in the transmission matrix data utilized. In the Level 1 optimization segment, the routine will use generalized data in the form of point value transmission matrices to determine the transmitted particle or

---

* Definitions of commonly used terms in these figures are given in Appendix A.

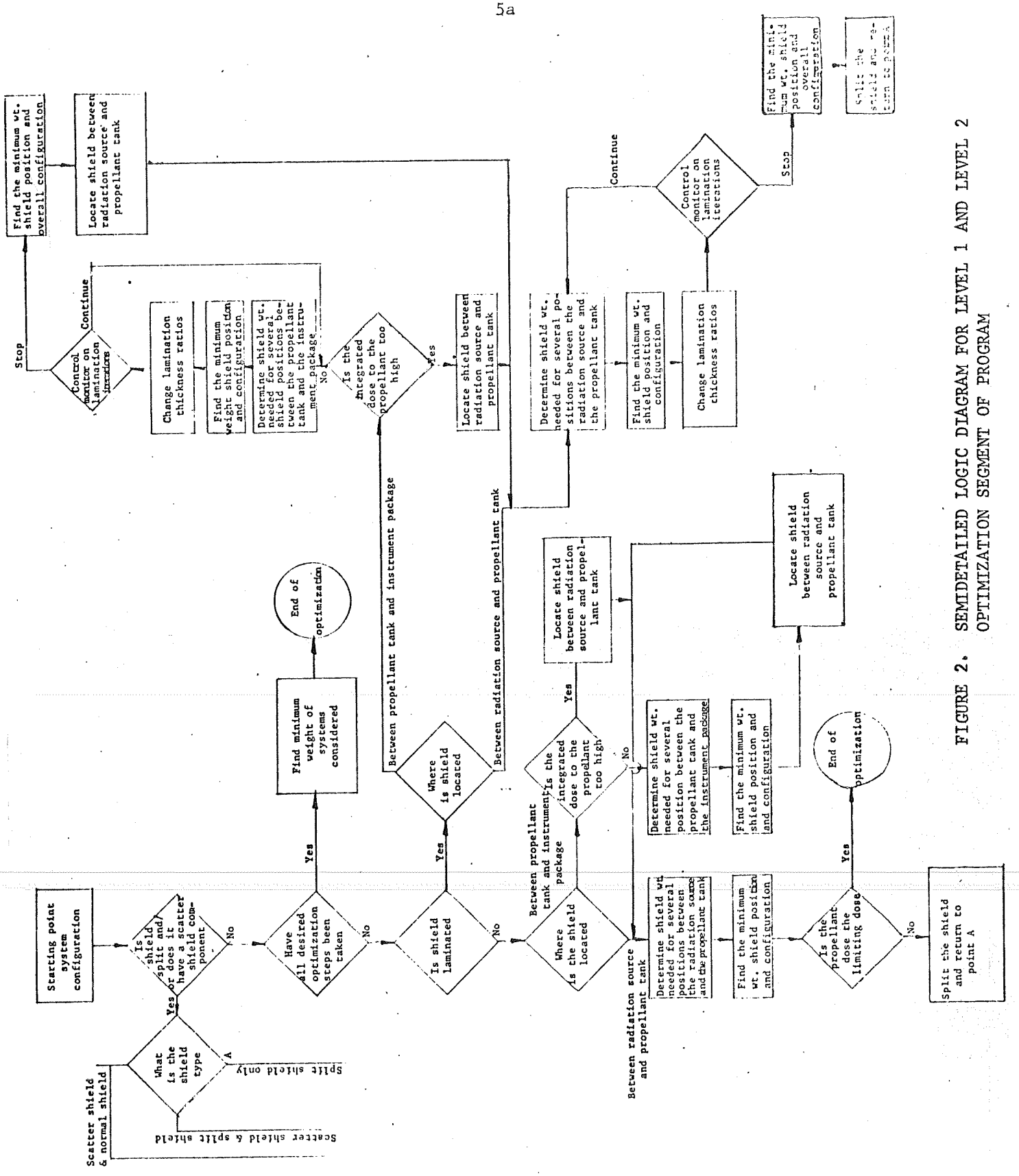

FIGURE 2. SEMIDETAILED LOGIC DIAGRAM FOR LEVEL 1 AND LEVEL 2 OPTIMIZATION SEGMENT OF PROGRAM

FIGURE 3. LOGIC DIAGRAM FOR LEVEL 1 OPTIMIZATION

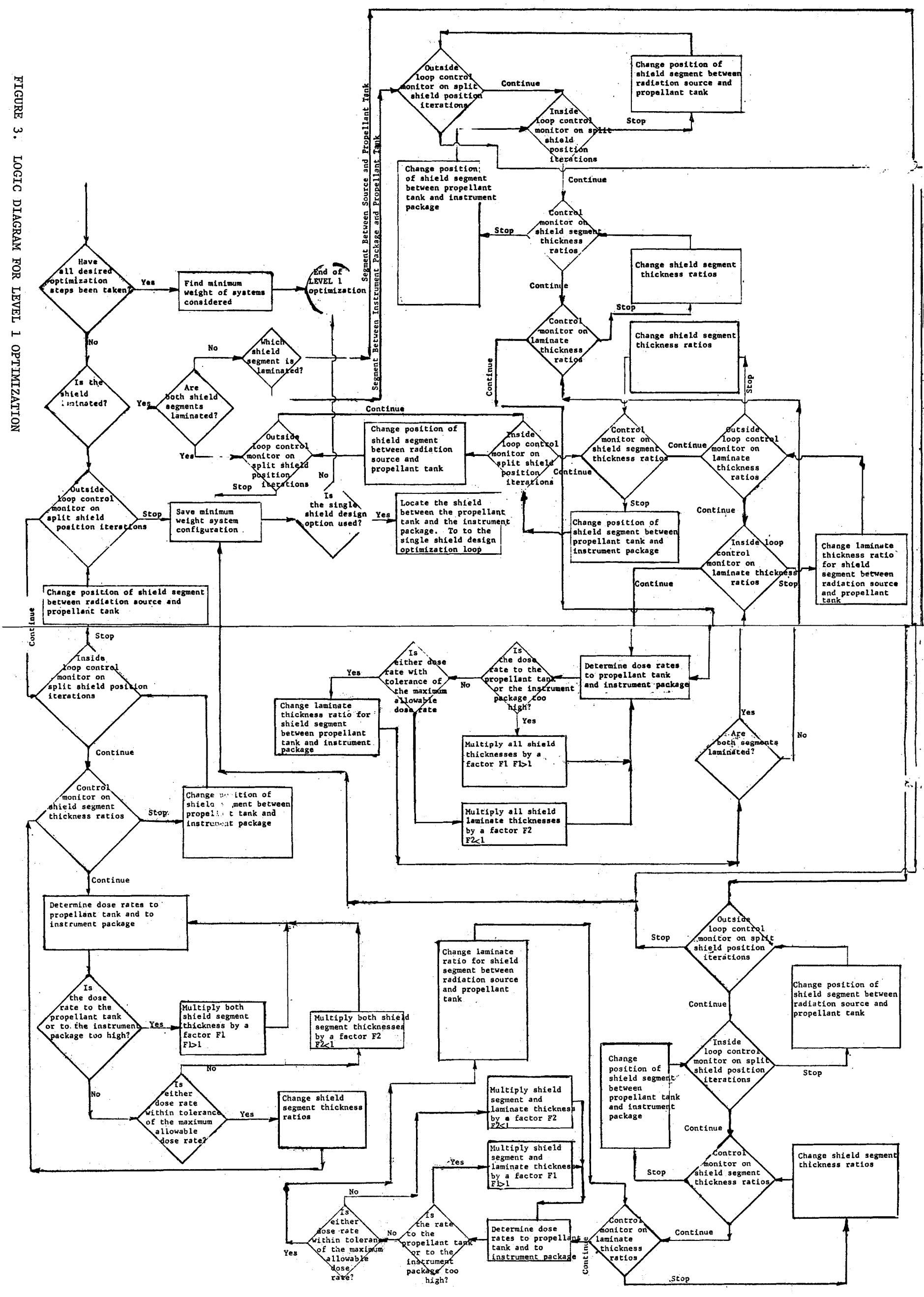

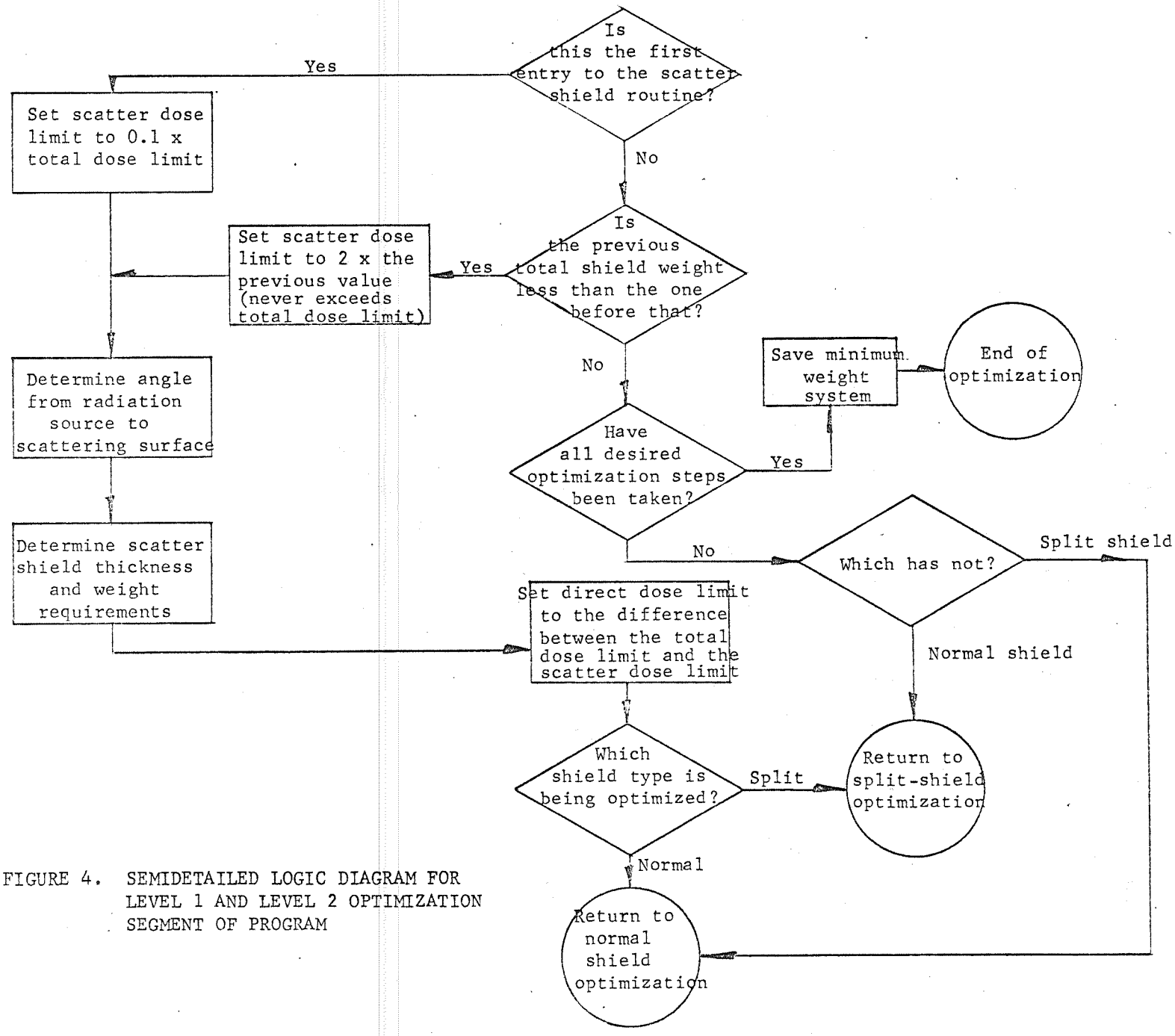

FIGURE 4. SEMIDETAILED LOGIC DIAGRAM FOR LEVEL 1 AND LEVEL 2 OPTIMIZATION SEGMENT OF PROGRAM

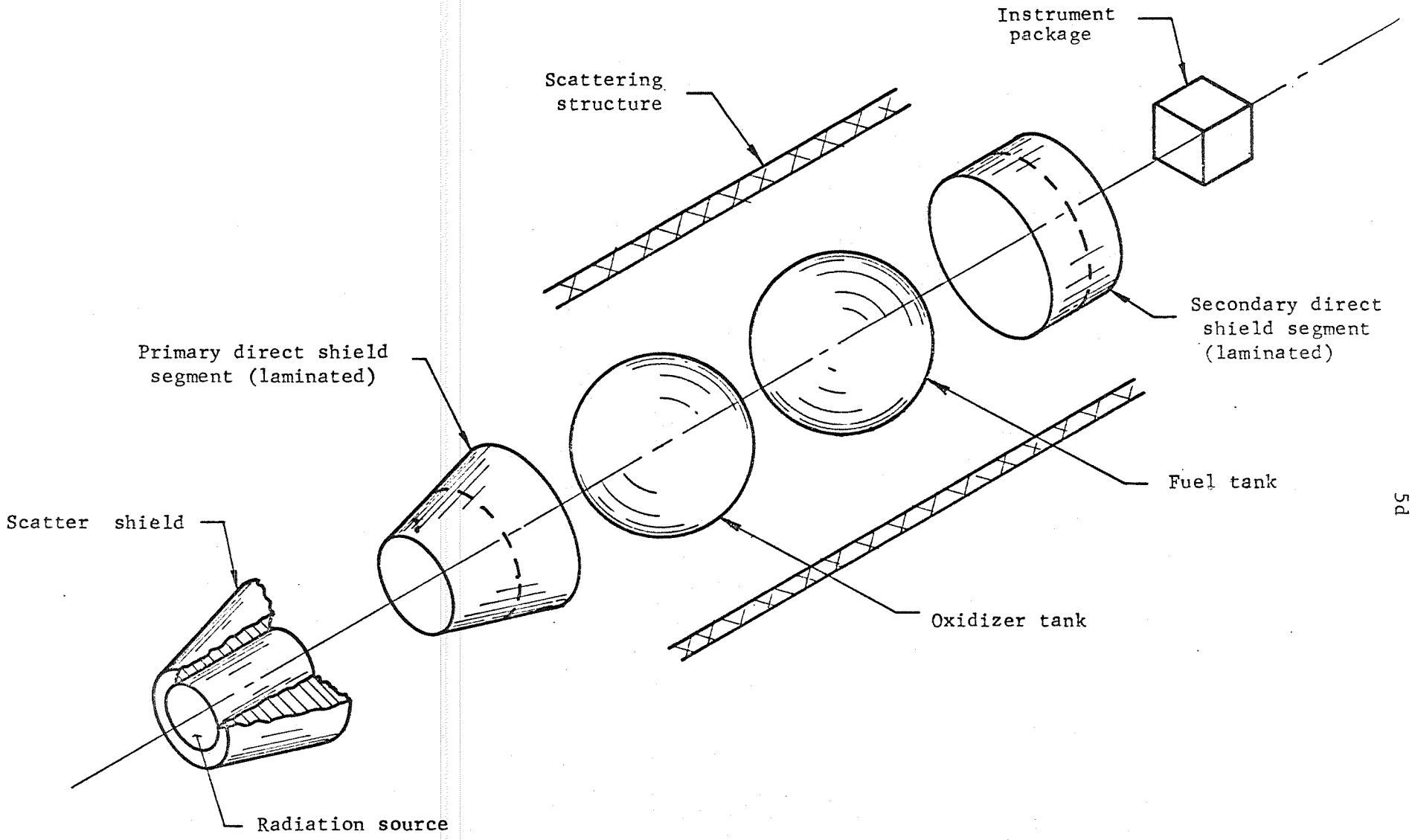

FIGURE 5. ANALYTICAL MODEL USED AS BASIS FOR PROGRAM LOGIC

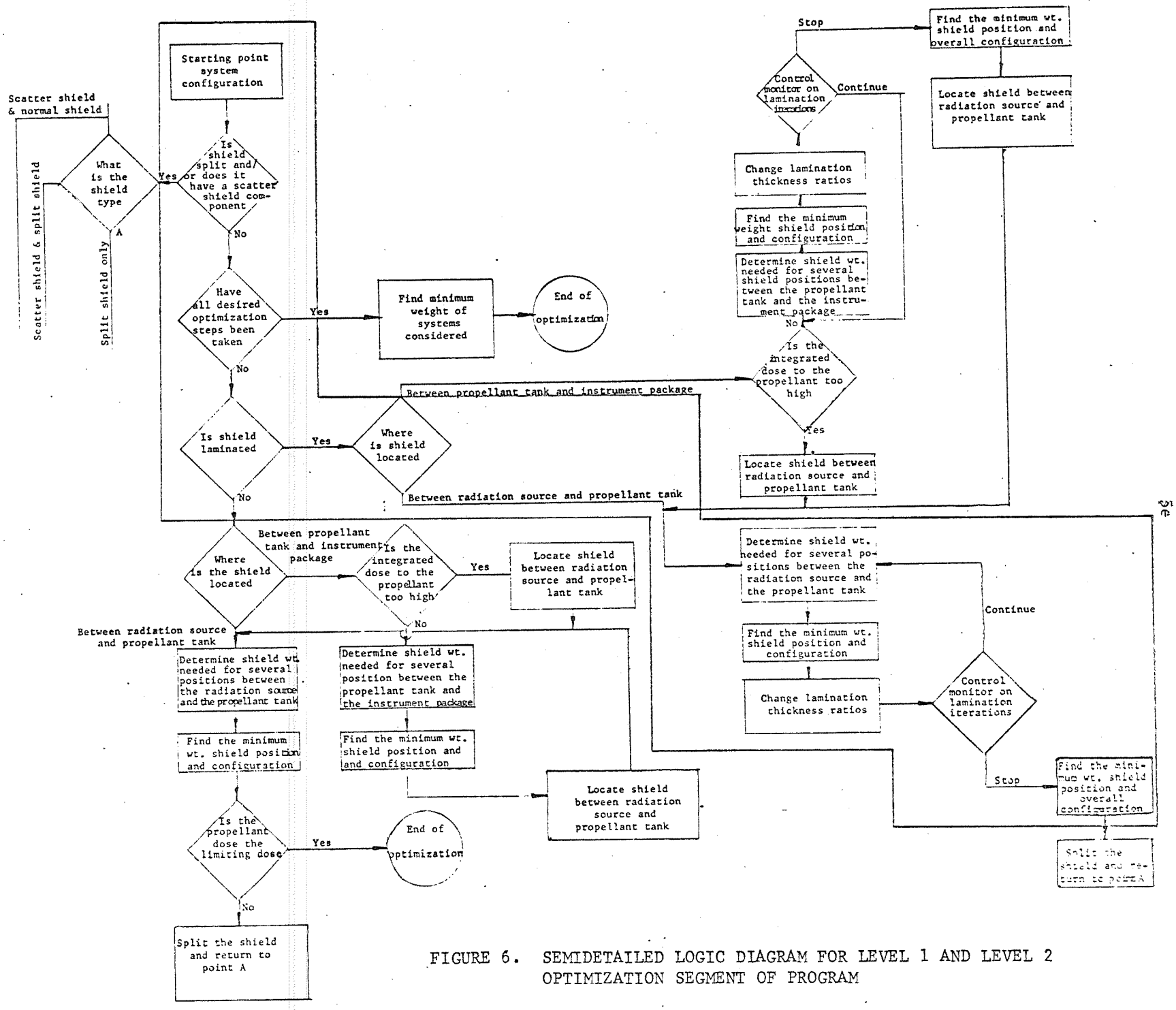

FIGURE 6. SEMIDETAILED LOGIC DIAGRAM FOR LEVEL 1 AND LEVEL 2 OPTIMIZATION SEGMENT OF PROGRAM

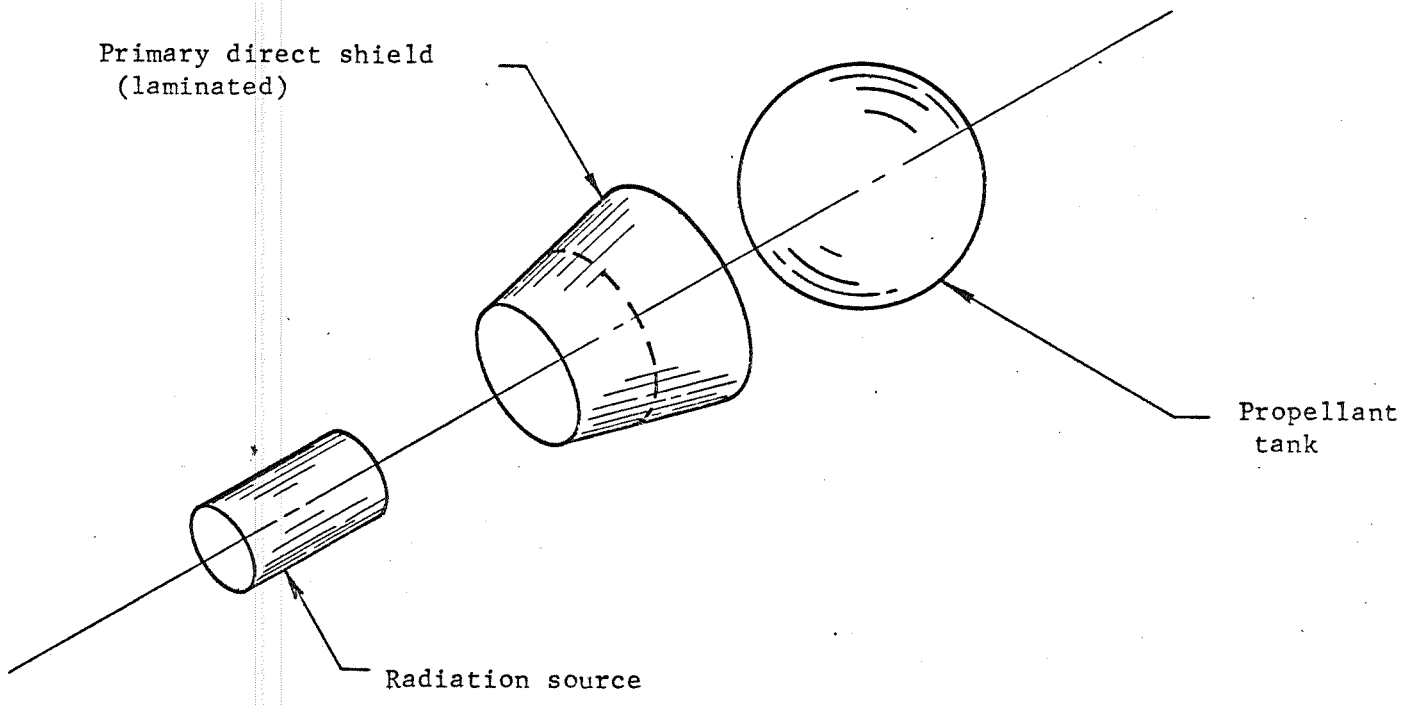

FIGURE 7. ANALYTICAL MODEL USED AS BASIS FOR PRELIMINARY PROGRAM

photon flux for each material traversed by the source radiation whereas, in the Level 2 optimization segment, the routine will rely on transmission matrices computed by another subroutine incorporated in the generalized optimization.

The routine as written will determine the optimum shield configuration for the system shown in Figure 7 which represents a portion of the analytical model shown in Figure 5.

Computer Program for the Optimization of "Primary Direct Laminated Shield"

A listing of the computer program which utilizes the transmission matrix technique is presented in Appendix C of this report. A sample problem input and output for this program is also listed.

SUMMARY OF TASK 2

Gamma-ray attenuation parameters for six candidate propellant constituents have been calculated. These data were then formulated into linear attenuation coefficients and buildup factors which have been presented in tabular form. A logic flow diagram for a generalized weight optimization computer program to select shielding configurations for propellant materials was generated. A simplified computer program which minimizes the weight of a primary direct laminated shield was developed. The program uses a transmission matrix solution technique, which reduces computation time, to calculate the radiation fluxes through the shield. Future work in this technical area should include (1) initiation of the programming of the generalized computer program to optimize the weight of space-shield propellant systems and (2) formulation of transmission matrices for use with the optimization technique.

RADIATION EFFECTS

Tasks 1 and 3

Experiments to obtain radiation effects data on Tasks 1 and 3 are described in this section of the report. Task 1 is radiation effects on several selected fuels and oxidizers as liquids while Task 3 is a Phase 1 storage test in a low dose rate radiation field. The liquid fuels examined in both tasks are hydrazine, diborane, and an LPG fuel, propane, and the liquid oxidizers are FLOX, oxygen difluoride, and nitrogen tetroxide, both inhibited and uninhibited forms. The results obtained from the two tasks are reported and discussed together in each fuel material category so that all information on a given material is together in a single section of the report.

Throughout this section of the report results are generally given in terms of G-values for gas formation resulting from irradiation. Radiation doses are given in rads. G-values are defined as the number of molecules of product formed per 100 ev of energy absorbed by the material in question. The unit of energy absorption, the rad, is defined as 100 ergs absorbed per gram of sample. The data are thus presented in a very general way so that the results can be easily applied to estimating radiation effects in other units such as pound-moles of product formed or gas pressure increase over a given amount of material for any volume and temperature. It is hoped that in this way the data obtained will be most useful to the largest number of people.

Experimental Procedures

Materials Handling

Two simple gas tight propellant handling systems were built and tested for the purpose of filling containers for irradiation experiments. One system was used for fuels and the other for oxidizers. Figures 8 and 9 are schematics of the propellant handling systems. Because of the corrosive nature of FLOX, OF_2, the other oxidizers studied on this program, all the fittings, gages, tubing, etc., of the oxidizer handling system are constructed of stainless steel, Monel, or nickel. The fuel system is of brass and stainless steel construction. Special care was taken in the cleaning and assembly of the components of the two systems to ensure removal of all contaminants, such as grease, moisture, oxide scale, etc., that might react violently on contact with oxidizers or fuels. The oxidizer system was passivated with fluorine gas which had been passed through an HF absorption tower before introducing FLOX or OF_2.

Each handling system contains a gas-measuring reservoir and pressure gage assembly of known volume so that a known amount of a propellant can be condensed into a precooled sample vessel for subsequent radiation effects experiments. The amount of propellant condensed may be controlled by successively filling the reservoir and transferring its contents to the sample vessel. After a desired percent fill is obtained, the sample vessel valve is closed and the liquid sample and coolant container is loaded into the container in which the radiation experiments will be conducted. The handling systems also include facilities for transferring and loading liquid propellants, such as N_2O_4 studied in Task 1 and Task 3 of this program.

Hydrazine (N_2H_4) is the only propellant not handled in these systems. Anhydrous hydrazine is transferred directly into the sample vessels using a calibrated syringe to measure the volume transferred. The transfer is done in a simple glovebox arrangement under a blanket of dry argon in order to prevent the hydrazine from picking up moisture.

FIGURE 8 FUEL LOADING SYSTEM

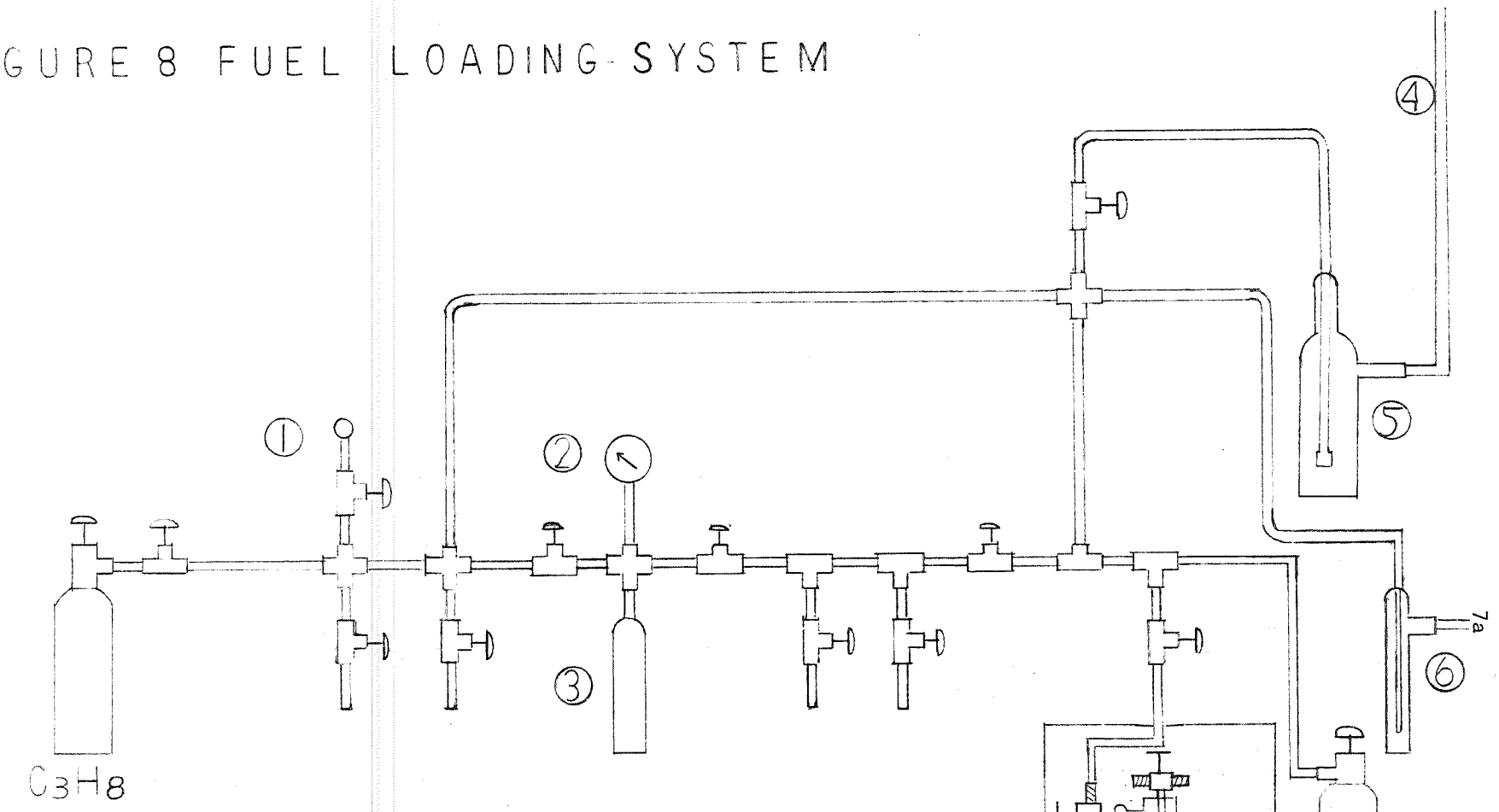

1. VACUUM GAGE
2. PRESSURE GAGE
3. MEASURING RESEVOIR
4. TO HOOD
5. WATER-METHANOL MIXTURE
6. COLD TRAP
7. NITROGEN CYLINDER
8. DIBORANE
9. DRY ICE

FIGURE 9 OXIDIZER LOADING SYSTEM

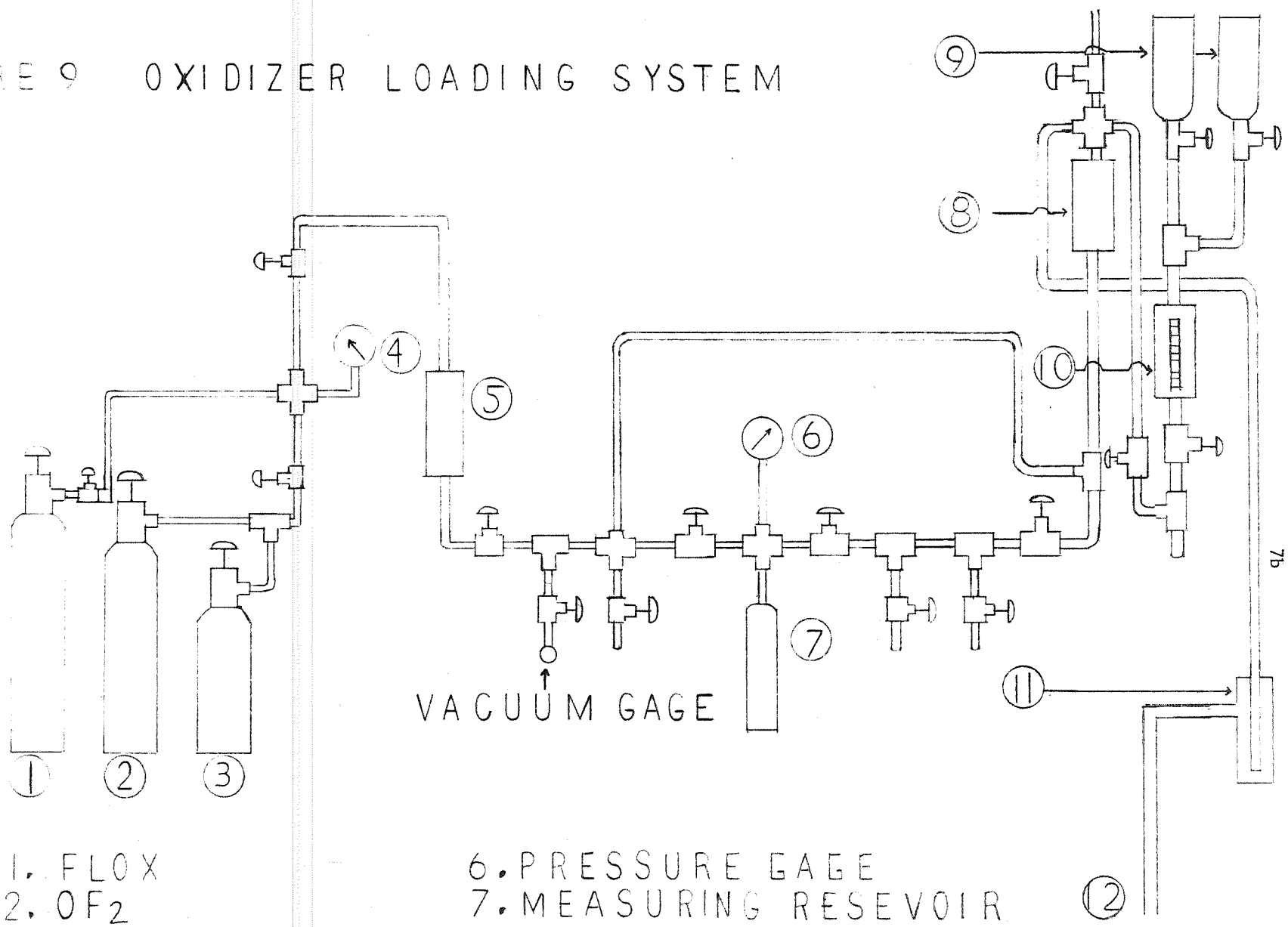

1. FLOX
2. OF_2
3. F_2
4. PRESSURE GAGE
5. HF ABSORBTION TOWER
6. PRESSURE GAGE
7. MEASURING RESEVOIR
8. SODA LIME TRAP
9. N_2O_4
10. CALIBRATED RESERVIOR
11. COLD TRAP
12. TO PUMP

An additional gas handling system was built and leak-checked and then used to obtain PVT data on any gas buildup in the irradiated samples and to obtain samples for mass spectrometric analysis of radiolytic products.

The fuel materials used in this study were analyzed by mass spectrometry prior to their use in radiation experiments.

FLOX. The fluorine-oxygen mixture was obtained from Allied Chemical and certified to be 70 ± 2 percent by weight fluorine. Our analysis by mass showed it to be quite pure. There was nitrogen present which could well have entered when we filled the sample vessel. A trace of hydrogen was observed. Some of the mass 28 peak could be due to CO since a peak was observed at mass 12.

Oxygen Difluoride. This material was obtained from Allied Chemical. Several analyses have been made and the purity is about 99 percent. There is a small amount of CO and HF present but their total quantity does not exceed 1 percent. Nothing else was found in these samples.

Nitrogen Tetroxide. The liquid N_2O_4 was obtained from Air Products and Chemicals, Inc., and was found to be at least 99 percent pure. There was evidence of a small amount of NO and perhaps a trace of water. Nothing else was found and total impurity content was less than 1 percent.

Diborane. The manufacturer, Callery Chemicals, claims the material's purity to be in excess of 98 percent and our analysis confirmed this. There is considerable nitrogen present which is to be expected, since nitrogen is generally used to pressurize the tanks. A small amount of hydrogen was also found and evidence of trace quantities of higher molecular weight boranes.

Hydrazine. Anhydrous hydrazine was obtained from Olin Matheson and found to have purity >99 percent. Significant amounts of argon were found as a result of our procedure of filling the sample vessels under a dry argon blanket. Water was present as a trace constituent as was ammonia. There was a small amount of mass 28 which could be either N_2 or CO.

Propane. This material was obtained from Air Products and found to be in excess of 99 percent pure. Only trace amounts of methane and ethane were found by mass analysis.

Sample Vessels

The sample vessels for containing the condensed propellants for Task 1 and Task 3 radiation experiments are all of the same simple basic design shown in Figure 10 but several materials were used. Some were constructed using a Hoke 2HS10-305SS sample cylinder, a 7-inch-long 1/4-inch 304SS high pressure tube extension, and a Hoke 1212G4Y valve for closure. Other vessels of the same type were made of Ti-6Al-4V alloy for use with hydrazine and N_2O_4 in particular. Further, some experiments were conducted with hydrazine and propane in 1100 F aluminum vessels of the same design and dimensions as shown in the figure.

Containers of 6063-T6 aluminum pipe construction in which the sample vessels were placed for carrying out radiation experiments at subambient and ambient temperatures in the Battelle gamma Co-60 radiation facility (swimming pool type) were built as shown schematically in Figure 11. A simple automatic liquid-nitrogen fill control system was constructed for Task 1 and Task 3 radiation experiments conducted at liquid nitrogen temperature and extending over considerable periods of time. In these cases a Dewar was placed in the containers to hold the irradiation vessels in a liquid nitrogen bath. The containers were connected to the liquid nitrogen supply through rubber tubing insulated by two 1/2-inch-thick lengths of Armflex insulating hose. This provided needed flexibility for inserting and removing the containers with sample vessels from the radiation source. Two thermistors were placed in the containers to sense liquid nitrogen levels. The lower thermistor would automatically start the fill cycle if the nitrogen fell below a predetermined level. The upper thermistor stopped nitrogen flow when the Dewar was filled. Flow was controlled by Asco solenoid valves. A timer was built into the circuit to periodically add nitrogen to the Dewar even though the level had not fallen below that of the lower thermistor.

Cobalt-60 Sources and Dosimetry

Five Co-60 radiation sources were assembled and dosimetry measurements performed on each. The standard ferrous sulfate dosimeter was used. The dosimetry measurements were carried out in a physical setup identical to that which was used in the Task 1 and Task 3 radiation experiments. The dosimeter was placed within a steel vessel of the same shape and wall thickness as the sample containers and this was placed in the aluminum container for irradiation. Thus, the dose rate seen by the dosimeter is the same as that which was seen by the sample. The dose rates (rads/hour) measured for the five Co-60 assemblies were 6.0×10^5, 8.0×10^4, 5.8×10^3, 5.0×10^3, and 5.7×10^3. The latter three sources were used for the long-term Task 3 experiments. Corrections were made for source decay as the program progressed.

Cobalt-60 gamma radiation was used throughout the experiments since the radiation induced decomposition is, in general, independent of the nature of radiation and a function only of the amount of energy deposited in the fuel materials. Also, in an on-board situation, the major radiation to which a

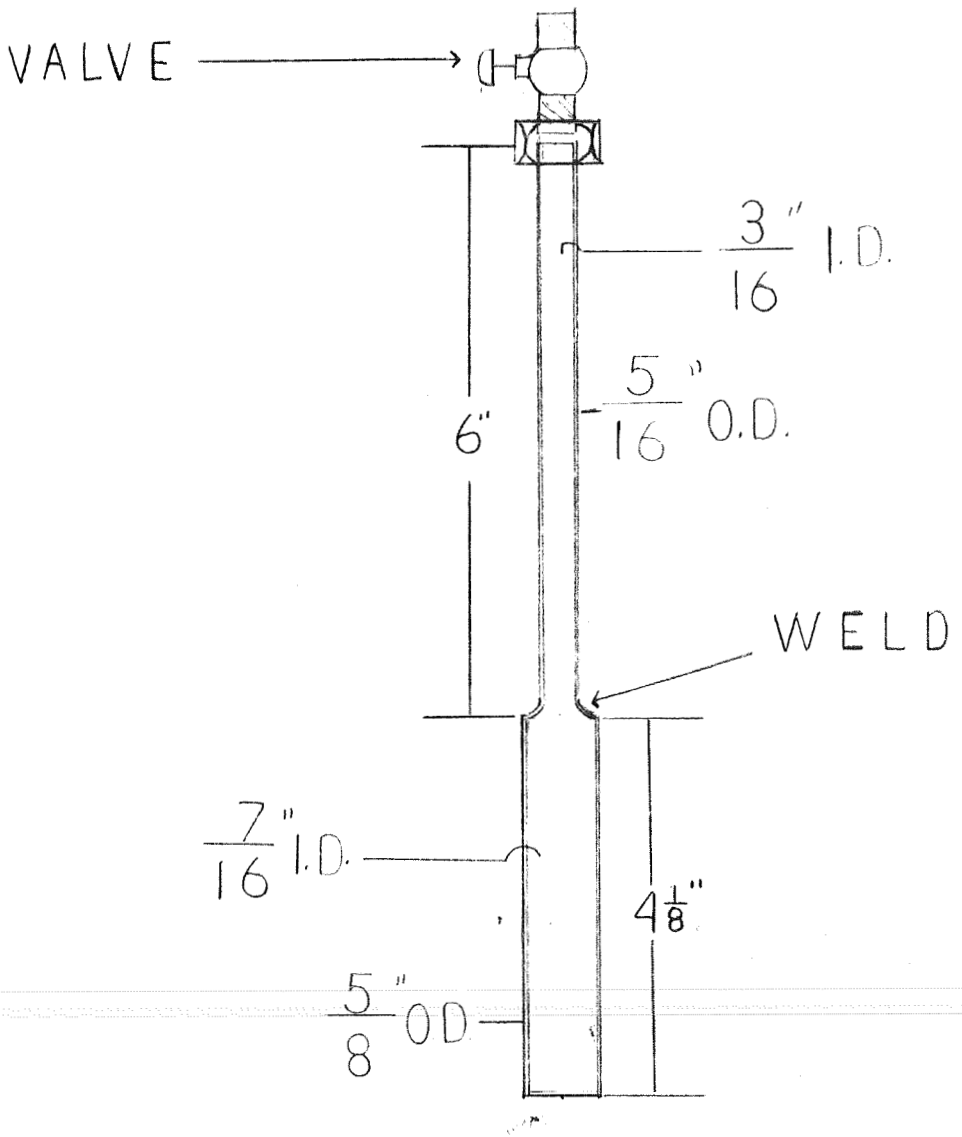

10 ML. CYLINDER

FIGURE 10 IRRADIATION VESSEL

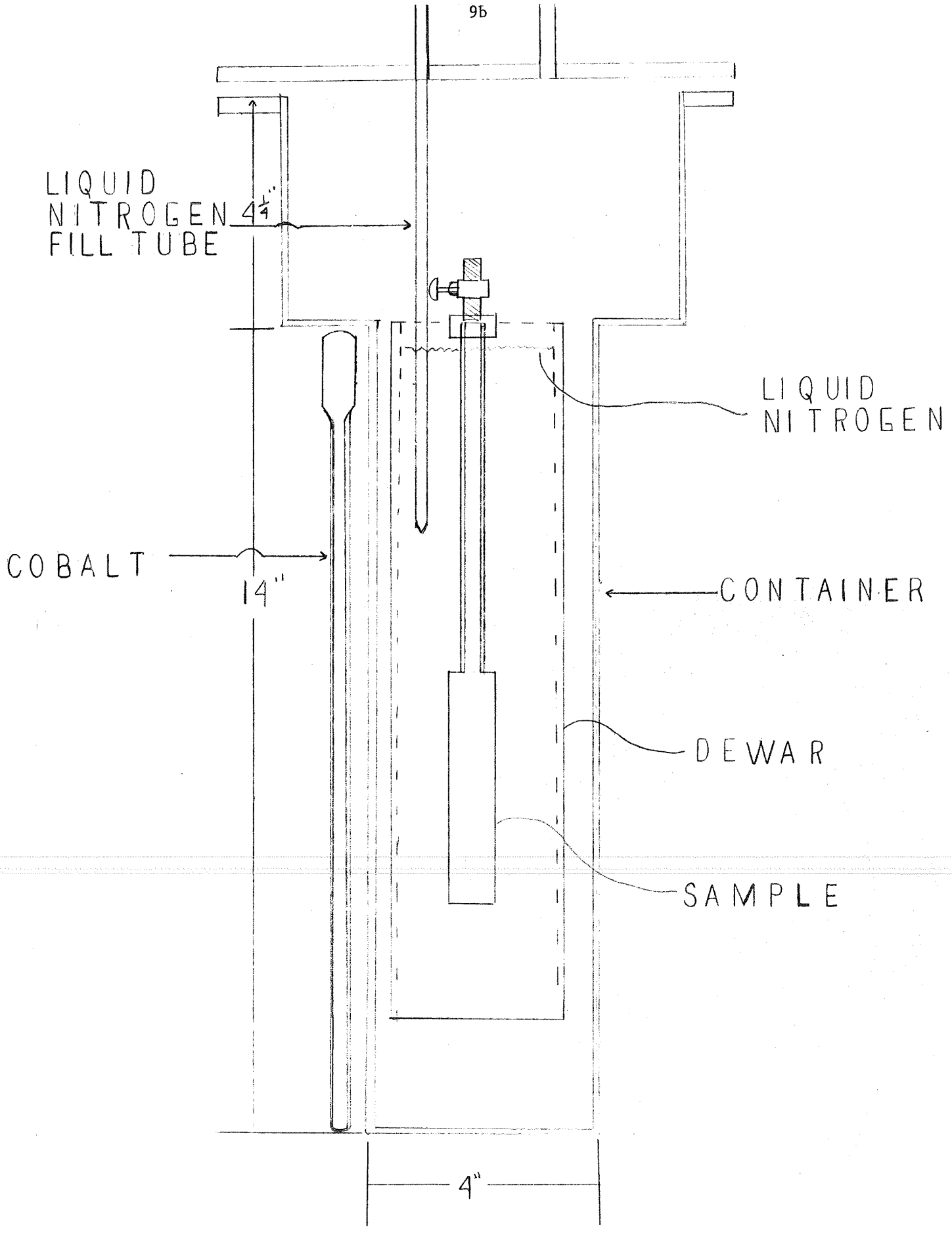
LIQUID
NITROGEN
FILL TUBE
4 1/4"
LIQUID
NITROGEN
COBALT
14"
CONTAINER
DEWAR
SAMPLE
4"

FIGURE II

fuel could be exposed may well be bremsstrahlung from the RTG. This is electromagnetic radiation of the same nature as gamma rays. Thus, the results generated here should be generally applicable regardless of the nature of RTG in an actual flight situation.

EXPERIMENTAL RESULTS

Diborane (B_2H_6)

A series of experiments were performed with diborane in stainless steel vessels. All irradiations were at -78.5 C and a dose rate of 5.87 x 10^5 rad/hr. In most cases the sample contained 1.31 gm of B_2H_6 liquid, or about 3 ml, which is about a 20 percent fill of the vessel. The vessels were filled using the system previously described.

The results of these experiments are given in Figure 12, where the moles of gas produced as a function of radiation dose is shown. The G-value for gas formation is $G(H_2)$ = 6.2 molecules/100 ev. This is equivalent to a gas buildup of about 0.14 ml/megarad. Assuming about one-half mole of gas is formed for each mole of diborane decomposed, the apparent rate of decomposition is about 0.04 percent per megarad.

These results are consistent with those of Cornelius, et al.,[2] who found hydrogen to be the only gaseous product formed. The overall rate of decomposition may be somewhat higher in our experiments, but this is difficult to ascertain accurately and probably not significant. The removal of a hydrogen atom from diborane would form an active species which would not be expected to remain long in the liquid without reaction. The products would be higher molecular weight borane compounds which will remain condensed under the conditions of these experiments. All such compounds might not be completely soluble but their rate of formation is probably not higher than that of hydrogen and hence their concentration is very low in these experiments.

To further check this point, additional experiments with liquid diborane were conducted in which mass spectrometric analysis was performed on both irradiated and unirradiated samples. As previously noted, the starting material is quite pure. In the vapor over the unirradiated liquid, B_2H_6 and a very small amount of H_2 were the only species observed. There were traces of B and BH which probably arise from electron impact in the ionization chamber of the spectrometer. The sample was then completely vaporized and an aliquot taken. Again, no species other than B_2H_6 and a small amount of H_2 were observed. The same procedure was followed with an irradiated sample. The noncondensible gaseous product observed was H_2. The irradiated sample was then completely vaporized and an aliquot analyzed. This showed B_4 compounds to be present which normally remain in the liquid when P-V-T measurements are made. These are the products expected from the dimerization of B_2H_6 fragments resulting from irradiation if, as expected, one of the major initial effects is removal of a hydrogen atom from diborane. That is:

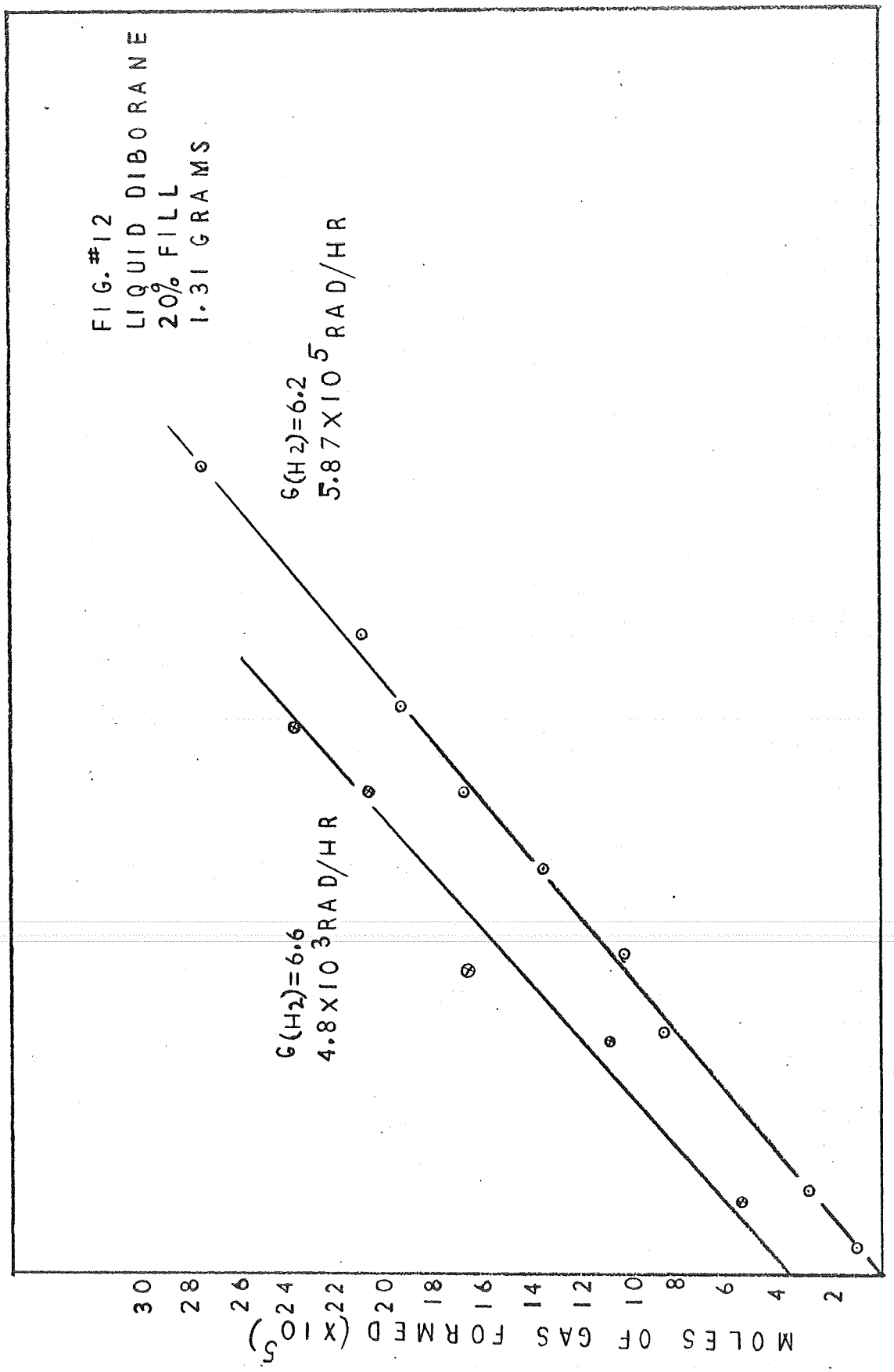
FIG. #12
LIQUID DIBORANE
20% FILL
1.31 GRAMS
G(H2)=6.2
5.87X10^5 RAD/HR
G(H2)=6.6
4.8X10^3 RAD/HR
MOLES OF GAS FORMED (X10^5)
DOSE, MEGARAD
2 4 6 8 10 12 14 16 18 20 22 24 26 28 30 32 34 36 38 40
2 4 6 8 10 12 14 16 18 20 22 24 26 28 30

$B_2H_6 \rightarrow B_2H_5 + H$

$B_2H_5 + B_2H_5 \rightarrow B_4$ compounds as products, and B_2H_6

$2H \rightarrow H_2$.

Other higher weight boron compounds would be expected to be formed in lesser amounts and this is also observed. The analysis showed a small amount of B_5 compound and a trace of B_3.

To simulate storage under low dose rate conditions an experiment was carried out involving irradiation for a period of about 6 months (4376 hours) at the same temperature and in the same type of container as used in the higher dose rate experiments. In these long-term experiments the average dose rate was approximately 4.8×10^3 rad/hr and the total exposure reached 22.2 megarad. The results of this experiment are also shown on Figure 12 where the result can be directly compared with those obtained at higher dose rates. It will be seen from the slopes of the lines that the apparent rate of radiation induced decomposition is not greatly different in the two cases and probably not significant, being 6.8 vs 6.2.

The curve for the low dose rate experiment does not go through the origin. The reason for this is not known. All sample preparation techniques were the same for the two sets of experiments. It is possible that the diborane warmed up during the 600 hours to reach the first data point. We do not know that this happened, but it is a possible explanation since thermal decomposition increases rapidly as the temperature approaches room temperature. Control samples were prepared and stored under identical conditions, with the exception of radiation, and these showed a gas formation rate that was only about 10 percent that of the irradiated samples. However, the significant point is that the slopes of the two lines are essentially the same since this is a measure of the decomposition rate as a function of absorbed energy. Thus there does not appear to be any effect of dose rate over the range investigated in these experiments.

An additional factor came to light too late in the program to be pursued in the data of Faust, Gould, and Kolman as reported in U.S. Patent 3,001,920.[3] Although the technical data revealed is limited, it suggests that a higher conversion of diborane to products was observed by them than observed in our experiments over the same range of doses. However, apparently all of their experiments were done at temperatures from 0 to 40 C or possibly higher, whereas ours were at -78 C. This suggests there may be a significant temperature effect on the rate of conversion of diborane to products in a radiation field. This point should be investigated in any future work with this fuel.

Propane (C_3H_8)

Propane was chosen as the LPG fuel material of interest. This choice was made after discussions involving several NASA scientists as explained in a letter to the project technical manager, May 6, 1969. Briefly, although there is considerable interest in methane as LPG fuel, there is also considerable detailed radiation effects data on methane. Propane, on the other hand, is also of interest as a fuel but there is, to our knowledge, no published radiation effects data on the liquid. Thus, it appears that, for this program, propane is the material which should be investigated.

In summary, the most recent and complete work on liquid methane is that of H. A. Gillis.[4] He worked with the liquid at 112 K (-116 C) and used Co^{60} for the source of gamma radiation. The irradiations were carried to about 0.12 percent methane decomposition. The loss of methane per unit dose was given as $G(-CH_4) = 6$ molecules/100 ev. This is approximately 0.01 percent decomposition per megarad.

The major products were hydrogen (H_2) and ethane (C_2H_6) which together account for about 95 percent of the observed products. Propane (C_3H_8) was about 4 percent of the product and all other higher hydrocarbon products accounted for less than 1 percent of the total. The rate of their formation per unit of absorbed radiation is given by their G-values, listed below.

$G(H_2)$	3.15
$G(C_2H_6)$	2.21
$G(C_3H_8)$	0.23
G(butanes)	0.037
G(all others)	0.012

Other radiation studies of methane have dealt primarily with the gas and have covered a range of temperatures in some detail up to 150 C, e.g., Bone and Firestone[5], and Sieck and Johnson[6]. Several other pertinent references are given in our report under NAS7-577, References 2-6.

Experiments with liquid propane at high and low dose rates were initiated using the same general filling and handling procedures described previously. The irradiation vessels were filled in the usual manner using Ti-6Al-4V capsules of approximately 15 cc volume. All irradiations were at dry ice temperature. The short-term samples utilized a dose rate of about 5.76×10^5 rad/hr and the long-term experiments were at a dose rate of about 4.80×10^3 rad/hr. At various exposures the buildup of gaseous products was determined by P-V-T relationships. Additional experiments with propane at the higher dose rate were done in 1100 F aluminum vessels to see if there were any obvious effects attributable to container material.

The results of the experiments are shown in Figures 13 and 14. In Figure 13 the sample was irradiated at -78 C and measured at the same temperature. In Figure 14, results shown are for samples irradiated as before but measured with the sample frozen at -196 C. At the lower temperature the most

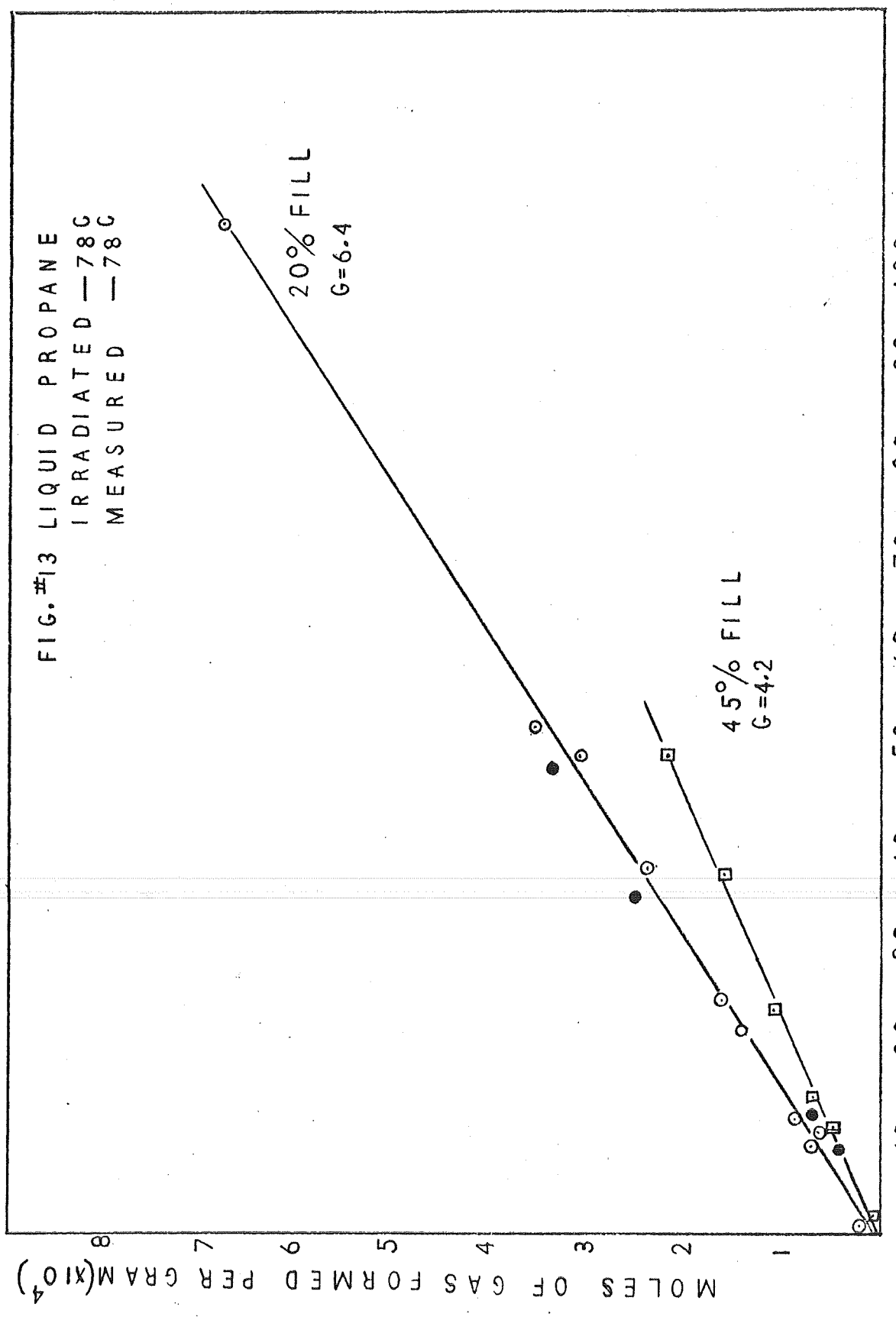
FIG. #13 LIQUID PROPANE
IRRADIATED —78C
MEASURED —78C
20% FILL
G=6.4
45% FILL
G=4.2
MOLES OF GAS FORMED PER GRAM(X10⁴)
DOSE, MEGARAD
1
2
3
4
5
6
7
8
10
20
30
40
50
60
70
80
90
100

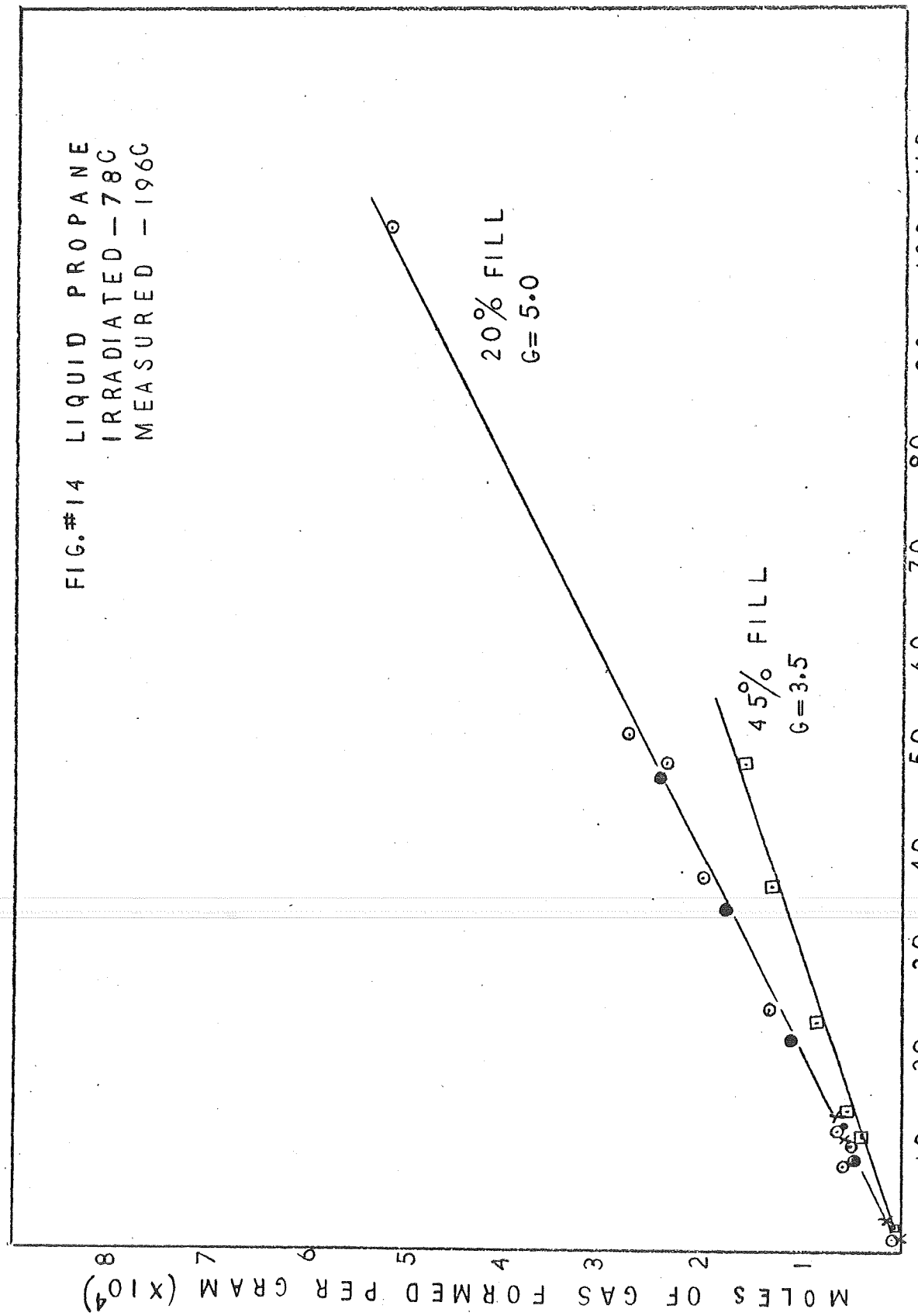
FIG.#14 LIQUID PROPANE
IRRADIATED — 78C
MEASURED — 196C
20% FILL
G= 5.0
45% FILL
G=3.5
MOLES OF GAS FORMED PER GRAM (X10⁴)
DOSE, MEGARAD
1
2
3
4
5
6
7
8
10
20
30
40
50
60
70
80
90
100
110

likely decomposition products expected to remain volatile are H_2 and CH_4. At the higher temperature, however, larger molecular species such as ethyl or butyl compounds would also be expected in the gas phase and would contribute to the total measured decomposition products. It is seen that apparent product yield as indicated by the G-value is 6.4 and 5.0 measured at -78 and -196, respectively.

From the figures it will also be noted that the yield per unit weight of irradiated sample is somewhat smaller when the vessel is more nearly full of liquid. This is true at both measuring temperatures and the ratio of the 20 percent filled (1.76 gm) to 40 percent filled (3.96 gm) is about the same in both cases. The explanation of this result is not known. The results suggest that the propane vapor is more susceptible to radiation induced decomposition than the liquid. However, much more work will have to be done to determine if this is indeed the case.

Samples of the gas above liquid propane at -78 C were analyzed by mass spectrometry. The results showed the major gaseous products to be unsaturated C_2 compounds, acetylene, and ethylene. Methane was also always present in significant quantities. The surprising result in these analyses was the general absence of hydrogen. From the amount of unsaturated compounds present there should have been easily discernible amounts of hydrogen. One might suspect that the hydrogen reacted with the titanium vessel in which the irradiation was performed. Such a reaction is less likely with an aluminum vessel, however, but there was no difference in the rate of product buildup when aluminum vessels were used. This can be seen in Figures 13 and 14 where part of the data points are open circles and others are filled circles. The open circles are data obtained in titanium and the filled circles are data from aluminum vessels. There are no significant differences in the two cases. Also, an experiment was done wherein a liquid propane sample was irradiated to 13.5 Mrad in a titanium vessel and the pressure followed for 98 hours after irradiation. No change was noted in the postirradiation period.

Low dose rate experiments were also conducted with liquid propane in the titanium vessels for a period of almost 4 months at an average dose rate of $4.8_0 \times 10^3$ rad/hr. These results are summarized in Figure 13 along with the data from higher dose rate experiments so that they can be compared directly. For the case of a 20 percent filled vessel the low dose rate data are indicated by crosses whereas the high dose rate data are shown by circles. The two sets of data fall on the same line indicating that the measured decomposition is function of the absorbed radiation dose but not the dose rate in this range.

Hydrazine (N_2H_4)

Preliminary radiation experiments with hydrazine in stainless steel vessels showed that considerable decomposition and gas buildup occurs. Anhydrous hydrazine (2.8 ml) was loaded under an argon atmosphere in a glove box into a 14.0-ml volume vessel. The sample was evacuated at -78.5 C through

several freeze-pump-thaw cycles to remove the argon and then irradiated at a dose rate of 6.0×10^5 rads/hour at room temperature for 118 hours. As calculated from postirradiation P-V-T data, a gas pressure buildup of 44 psia and a 1.6 percent decomposition of the hydrazine occurred at the conditions of the experiments. Mass spectrometric analysis of the sample at room temperature showed considerable amounts of H_2, N_2, and NH_3 with an estimated molar ratio of 6.8:4.3:1, respectively. The sample was then cooled to liquid nitrogen temperature, pumped on to remove the N_2 and H_2, and allowed to warm to room temperature. Relatively large amounts of ammonia (NH_3), which had been condensed while most hydrogen and nitrogen were removed, and trace amounts of H_2, N_2, and CO_2 were observed along with the hydrazine. No other radiolytic products were observed. Preceding the mass spectrometric analysis, vapor pressure measurements of the sample obtained at liquid nitrogen, Dry Ice, and room temperature tend to support the mass spectrometric data. The starting hydrazine sample had a vapor pressure of about 3 psia (150 mm of Hg) at room temperature and only trace amounts of nitrogen and CO_2 were observed by mass spectrometric analysis. Further, preliminary experiments with hydrazine in stainless steel vessels indicated significant decomposition which seemed to be a function of the surface. Lucien and Pinns[7] had observed a surface effect when irradiations were performed in Pyrex vessels. Also, the apparent decomposition in the vapor was much greater than in the liquid at corresponding doses.

A series of experiments was established for irradiating anhydrous hydrazine in Ti-6Al-4V vessels filled as described previously. All radiation exposures were at 22 C and a dose rate of $6.1_6 \times 10^5$ rad/hr. Several different sample volumes were used so that the liquid-vapor ratio was varied. Hydrazine vapor was the only gas present over the liquid during irradiation.

The results of these experiments are shown in Figure 15. The range of volumes of liquid samples was from 3 to 10 cc, which corresponds to 20 to 66 percent of the total vessel volume. The figure shows that formation of gaseous products not condensible at -78.5 C, i.e., N_2 and H_2, is unaffected by a change in ullage. The results are plotted as moles of gas formed per gram of sample as a function of dose to show that gas formation per unit of hydrazine is constant at the various gas-liquid ratios. The pressure buildup over the larger samples was of course greater. A larger mass of sample was being irradiated and the ullage was smaller leading to higher pressure.

The results shown in Figure 15 are reasonably consistant with what other data are available. The rate of gas formation at STP is about 0.1 ml/Mrad per gram of liquid hydrazine. In working with monomethyl hydrazine, which would be expected to give similar results, Shelberg[8] and Plank[9] both measured about 0.2 ml/Mrad. Lucien and Pinns give values between 0.1 and 0.7 with most falling around 0.2 ml/Mrad. These values correspond to decomposition rates of the order of 0.01 percent per megarad.

Based on volume of gas formed, our data give G = 5.8 (molecules of gas formed per 100 ev absorbed). Based on the gas volume data of Lucien and Pinns[7], we calculate $G \simeq 7$ for their experiments with liquid hydrazine irradiated in glass ampoules by X-rays. The nitrogen-hydrogen ratios quoted

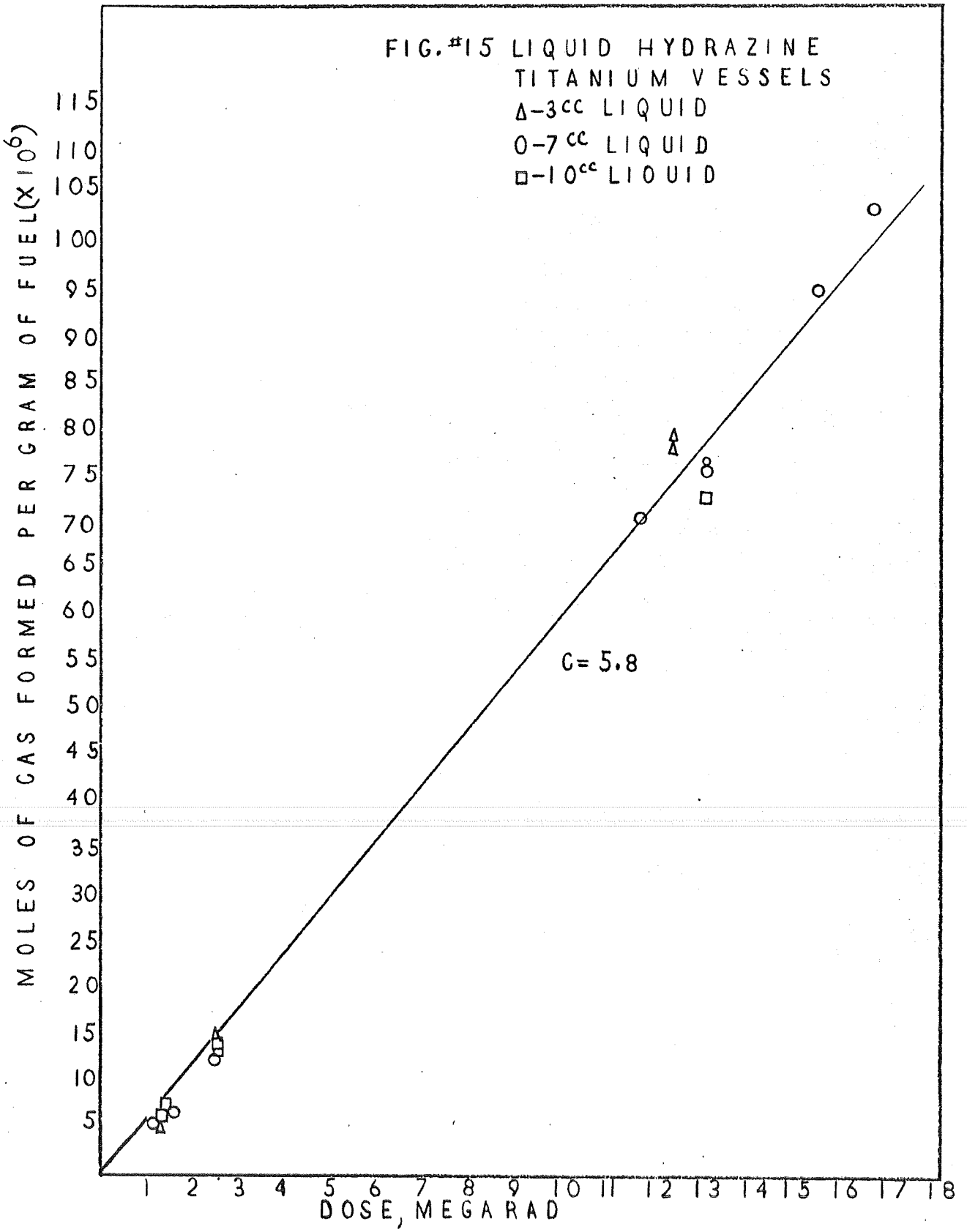
FIG. #15 LIQUID HYDRAZINE
TITANIUM VESSELS
Δ-3cc LIQUID
O-7 cc LIQUID
□-10cc LIQUID
C= 5.8
MOLES OF GAS FORMED PER GRAM OF FUEL(X10^6)
115
110
105
100
95
90
85
80
75
70
65
60
55
50
45
40
35
30
25
20
15
10
5
1 2 3 4 5 6 7 8 9 10 11 12 13 14 15 16 17 18
DOSE, MEGARAD

by them fall between 0.5 and 1.5 with most being 1.0 while our data give a value of about 1.5.

Although this agreement is reasonably good it does raise some questions. Lucien and Pinns quote G-values for hydrazine decomposition of the order of 2×10^2, which is difficult to reconcile with their gas release data. If hydrazine decomposes completely to nitrogen and hydrogen one would expect the gas ratio to be 0.5 and the G-value for decomposition to be one-third of that for gas formation, i.e.,

$$N_2H_4 \rightarrow N_2 + 2H_2 \quad .$$

However, if hydrazine predominately forms ammonia on decomposition the nitrogen-hydrogen ratio would be expected to be about 1 and the G-value for hydrazine decomposition would equal that for the formation of noncondensible gases, i.e.,

$$2N_2H_4 \rightarrow 2NH_3 + N_2 + H_2 \quad .$$

Our analyses have not shown large amounts of ammonia, nor apparently did those of Lucien and Pinns. This matter needs to be investigated in further detail.

An additional series of experiments was initiated with liquid hydrazine in aluminum vessels for comparison with previous results obtained with liquid hydrazine in titanium alloy vessels. The initial results had indicated some surface-related decomposition in stainless steel vessels but not in the titanium ones. The later experiments were conducted using the same procedures throughout with only the vessel material being different. All experiments were at $5.5_3 \times 10^5$ rad/hr and 22 C.

The results of these experiments using aluminum vessels are shown in Figure 16. The volume of liquid samples used was either 3 or 7 cc, which is equivalent to about 20 or 45 percent of the vessel volume. The figure shows the moles of gaseous products not condensible at -78.5 C, i.e., N_2 and H_2, as a function of radiation exposure. The products are given per unit weight of sample so that the two gas-liquid ratios for the different fillings can be directly compared. It is seen that decomposition, as determined by post-irradiation P-V-T measurements, is unaffected by a change in ullage. The G-value for gas formation is found to be 5.7_5 whereas the previously determined value in titanium vessels was 5.8_0. There is, therefore, no apparent difference between the two sets of data or the response to irradiation in the two types of vessels.

Low dose rate experiments were conducted at an average of about 5.6×10^3 rad/hr for approximately 189 days (4544 hours) and a total exposure of 24.9 Mrad in the titanium alloy vessels. These data are summarized in Figure 17. The rate of product formation is equivalent to a value of G = 7.7 which is significantly higher than in the high dose rate experiments in either type of vessel. Suitably stored control samples were maintained over the entire period of irradiation and the maximum increase in pressure in these

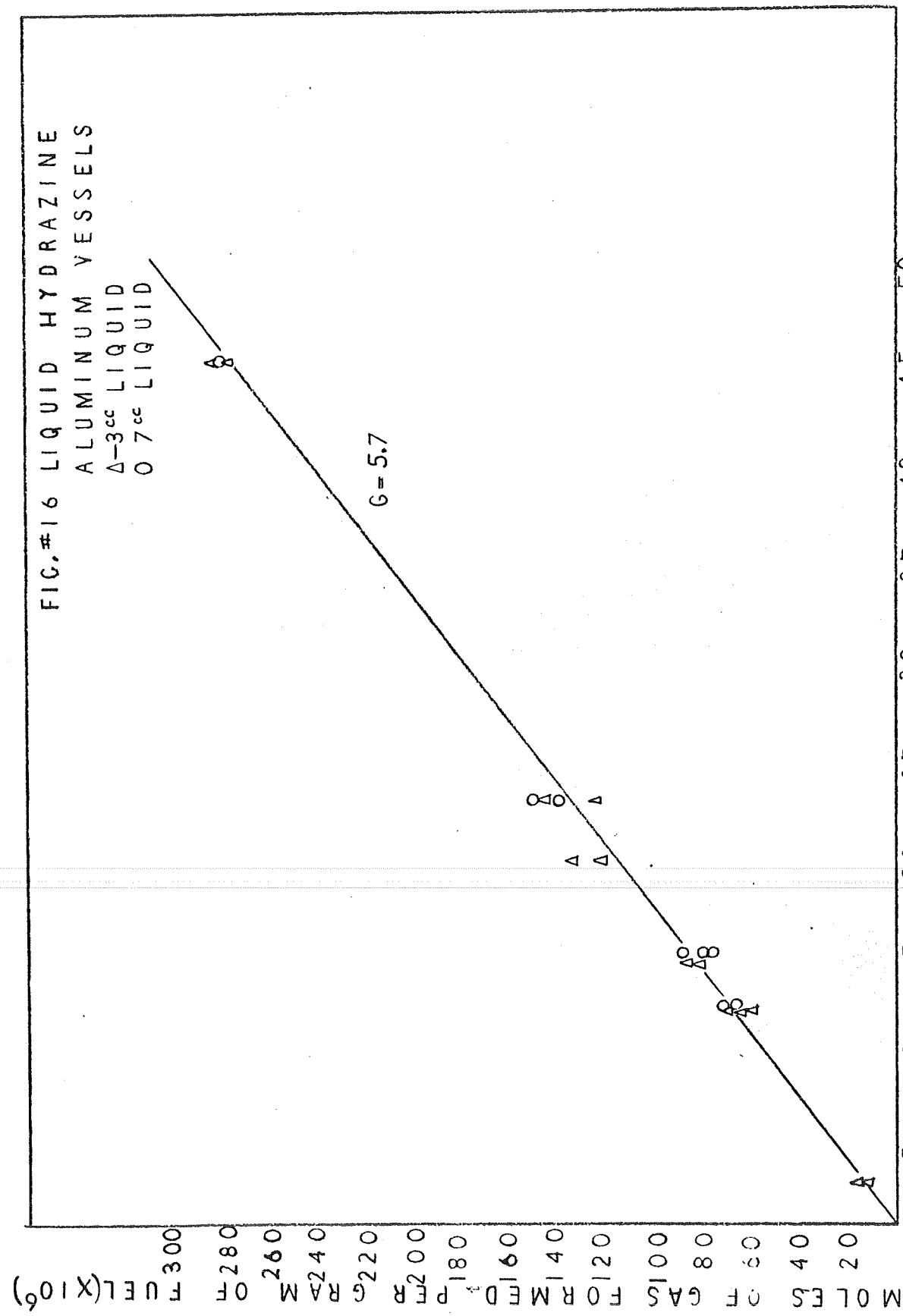
FIG. #16 LIQUID HYDRAZINE
ALUMINUM VESSELS
Δ—3cc LIQUID
O 7cc LIQUID
G = 5.7
MOLES OF GAS FORMED PER GRAM OF FUEL(X10⁶)
DOSE, MEGARAD
20
40
60
80
100
120
140
160
180
200
220
240
260
280
300
5
10
15
20
25
30
35
40
45
50

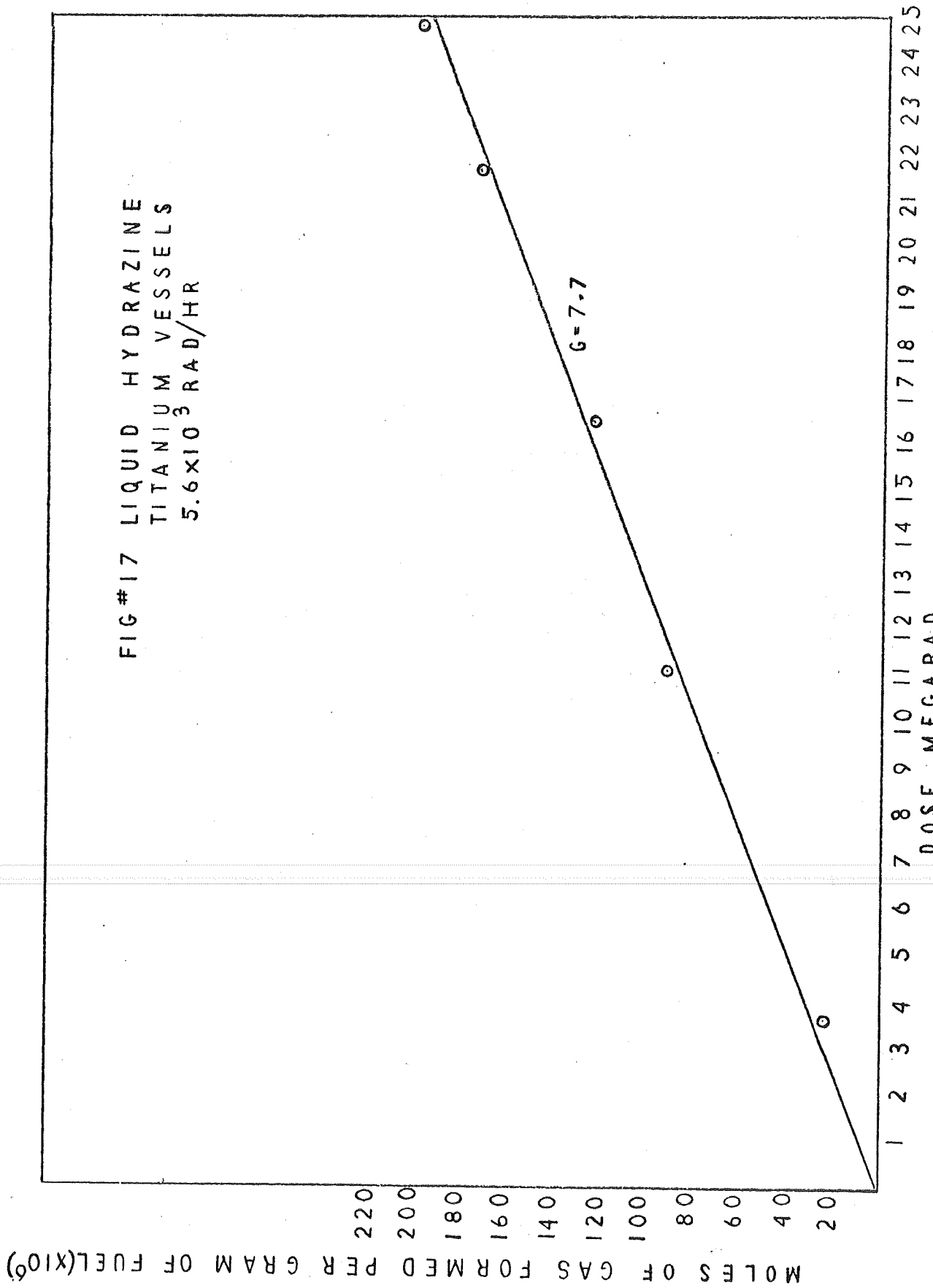
FIG #17 LIQUID HYDRAZINE
TITANIUM VESSELS
5.6×10³ RAD/HR
G=7.7
MOLES OF GAS FORMED PER GRAM OF FUEL(X10⁶)
20
40
60
80
100
120
140
160
180
200
220
1 2 3 4 5 6 7 8 9 10 11 12 13 14 15 16 17 18 19 20 21 22 23 24 25
DOSE, MEGARAD

was less than 10 percent of the corresponding irradiated sample. The results were corrected for this nonirradiation pressure rise but it is apparent that a factor of this nature cannot account for the difference between the high and low dose rate experiments. The reason for the difference is not known and it does appear real. It is a point that should be considered in more detail in future work.

FLOX ($O_2 + F_2$)

Experiments with liquid FLOX were conducted in stainless steel vessels at liquid nitrogen temperature at a dose rate of $5.7_6 \times 10^5$ rad/hr for a total exposure of 22.6 Mrad. The samples were prepared using the oxidizer handling facility and techniques previously described. The long-term tests with this oxidizer were allowed to progress for about 5000 hours. These samples received approximately 25 Mrad exposure. In none of these experiments have we seen any effect attributable to irradiation. This is not an unexpected result. The materials involved, liquid oxygen and fluorine, are stable compounds and any reaction initiated by the radiation would probably be small. The products of such reaction, perhaps OF_2, would be present at low concentration, soluble in the liquid, and contribute very little to the vapor pressure of the sample. Due to the lack of observable effects, these experiments were carried no further.

Oxygen Difluoride (OF_2)

All short-term experiments with liquid oxygen difluoride were performed at a dose rate of $6.0_0 \times 10^5$ rad/hr in stainless steel vessels and at a temperature of -196 C. Samples were loaded into the vessels using the previously described handling system and pressure over the liquid was determined. Each vessel contained 5.0 gm of OF_2 liquid which filled about 20 percent of the available volume. After the appropriate irradiation, the pressure was again determined at -196 C and the moles of gaseous products formed were ascertained from P-V-T relations.

The results of these experiments are shown in Figure 18 where the moles of gaseous decomposition products, O_2 and F_2, are shown as a function of radiation dose. It will be noted that in this case the yield of decomposition products is not linear with dose as were the fuels. The fact that the yield is not constant but decreasing probably indicates a secondary reaction which is removing the gaseous products at a slow but definite rate. One such reaction which immediately suggests itself is the reaction of O_2 and F_2 gas to reform OF_2 liquid, i.e.,

$$1/2\ O_{2(g)} + F_{2(g)} \rightarrow OF_{2(l)} \quad .$$

It is also possible that some O_2F_2 could be formed which would also condense at the temperature of these experiments and lead to an apparent decrease in the rate of decomposition of OF_2.

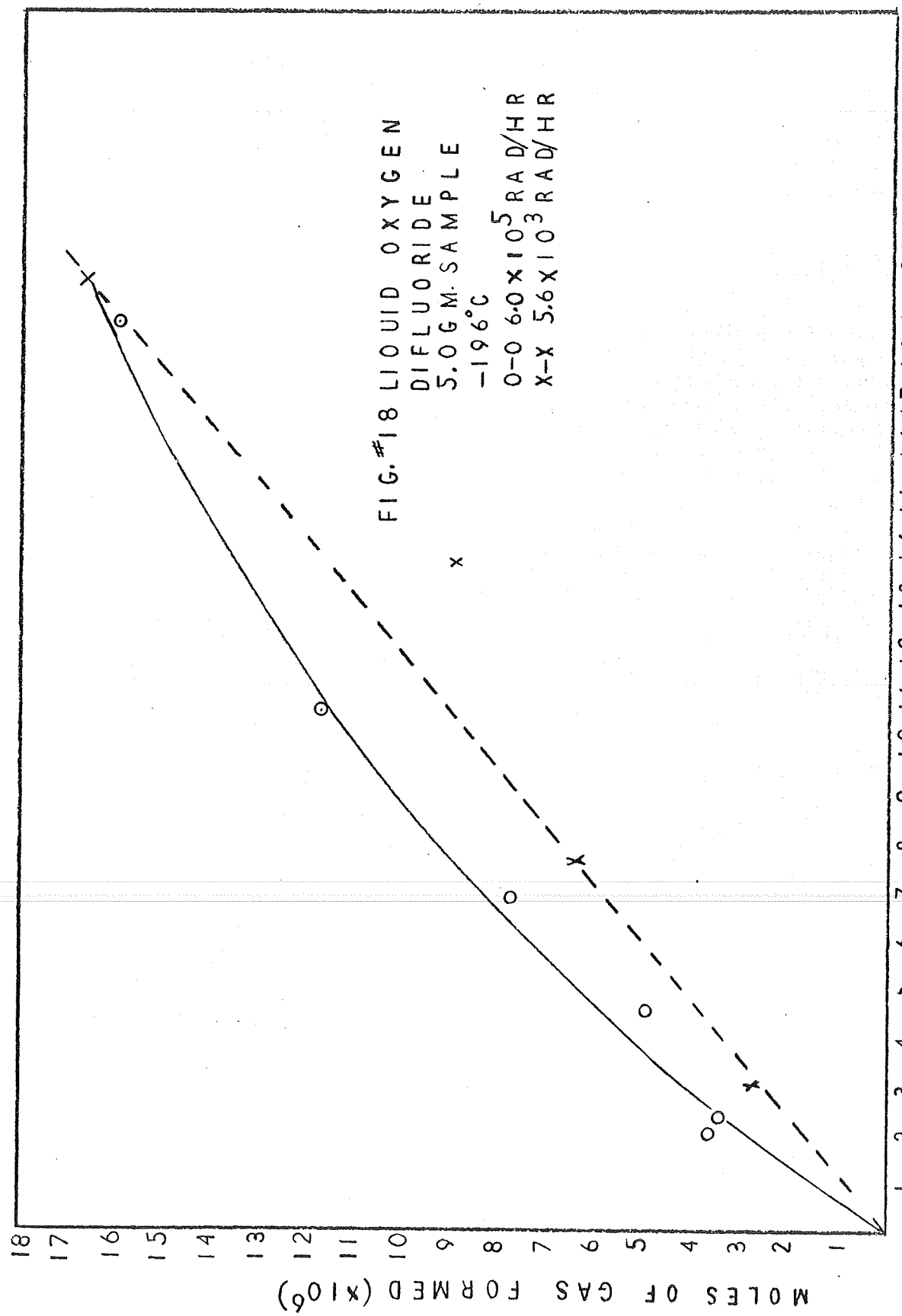
FIG. #18 LIQUID OXYGEN
DIFLUORIDE
5.0 G M. SAMPLE
-196°C
O–O 6.0 X 10^5 RAD/HR
X–X 5.6 X 10^3 RAD/HR
MOLES OF GAS FORMED (X10^6)
DOSE, MEGARAD
1 2 3 4 5 6 7 8 9 10 11 12 13 14 15 16 17 18 19 20
1 2 3 4 5 6 7 8 9 10 11 12 13 14 15 16 17 18

Since the rate of formation of decomposition products, and hence the G-value, decreases with increasing dose, the value at low doses is most important since that gives the maximum value and indicates the maximum rate of radiation induced decomposition. The initial value is G(gas) = 0.30 molecules/100 ev. A G-value this low indicates liquid OF_2 is rather radiation resistant. The data further indicate a maximum gas buildup rate of about 6.9×10^{-3} ml/megrad. Assuming one and a half molecules of gaseous product for each molecule of liquid OF_2 decomposed, G-(OF_2) = 0.20 molecules/100 ev. This is equivalent to about 1×10^{-3} percent decomposition per megarad.

Long-term experiments were extended for a period of almost nine months. However, after about five months we began to experience difficulty with leaking valves on the sample vessels so that the data after that were not reliable. As can be seen from Figure 18, the rate of buildup appears more linear at 5.6×10^3 rad/hr than at the higher dose rate. However, the amount of decomposition is always very small in all experiments and the differences in the two cases are probably not significant and using an overall value of G(gas) = 0.17 for the whole range of dose rates is justified.

Nitrogen Tetroxide (N_2O_4)

Experiments with liquid nitrogen tetroxide were conducted by the same general procedures outlined previously. Stainless steel vessels of approximately 15 cc were used. Irradiations by Co-60 were performed at a dose rate of $5.7_6 \times 10^5$ rad/hr and a temperature of 21 C. Sample vessels were evacuated prior to filling with N_2O_4. After filling, the liquid N_2O_4 was frozen and any noncondensible gases removed by pumping. Noncondensible gases at liquid N_2 temperature formed by decomposition of N_2O_4 were determined as a function of time and radiation dose by P-V-T relationships.

The results of experiments at the dose rate of $5.7_6 \times 10^5$ rad/hr for both the uninhibited and inhibited forms of N_2O_4 are shown in Figures 19 through 22 as moles of noncondensible gas formed per gram of liquid N_2O_4 as a function of radiation dose. Several points are immediately obvious from these figures; the inhibited form shows more apparent radiation decomposition at a given radiation exposure; the scatter in the data, particularly at the lower filling (3-cc sample), is greater than in many of our other experiments; and the decomposition rate at a fixed dose rate appears to be a function of the extent to which the sample vessel was filled. A 3-cc sample fills the sample volume approximately 20 percent while a 10-cc sample fills it about 67 percent.

These results suggest that the vapor is more susceptible than the liquid to decomposition and that there is some interaction with the walls of the vessel. Several other observations are consistent with this. The amount of noncondensible gas formed, largely N_2, in unirradiated control samples was also a function of the filling, being between about 1 and 20 percent of the radiation induced decomposition product for the 3-cc samples, and 2 percent or less in those samples with 7 or 10 cc of liquid N_2O_4. The magnitude of

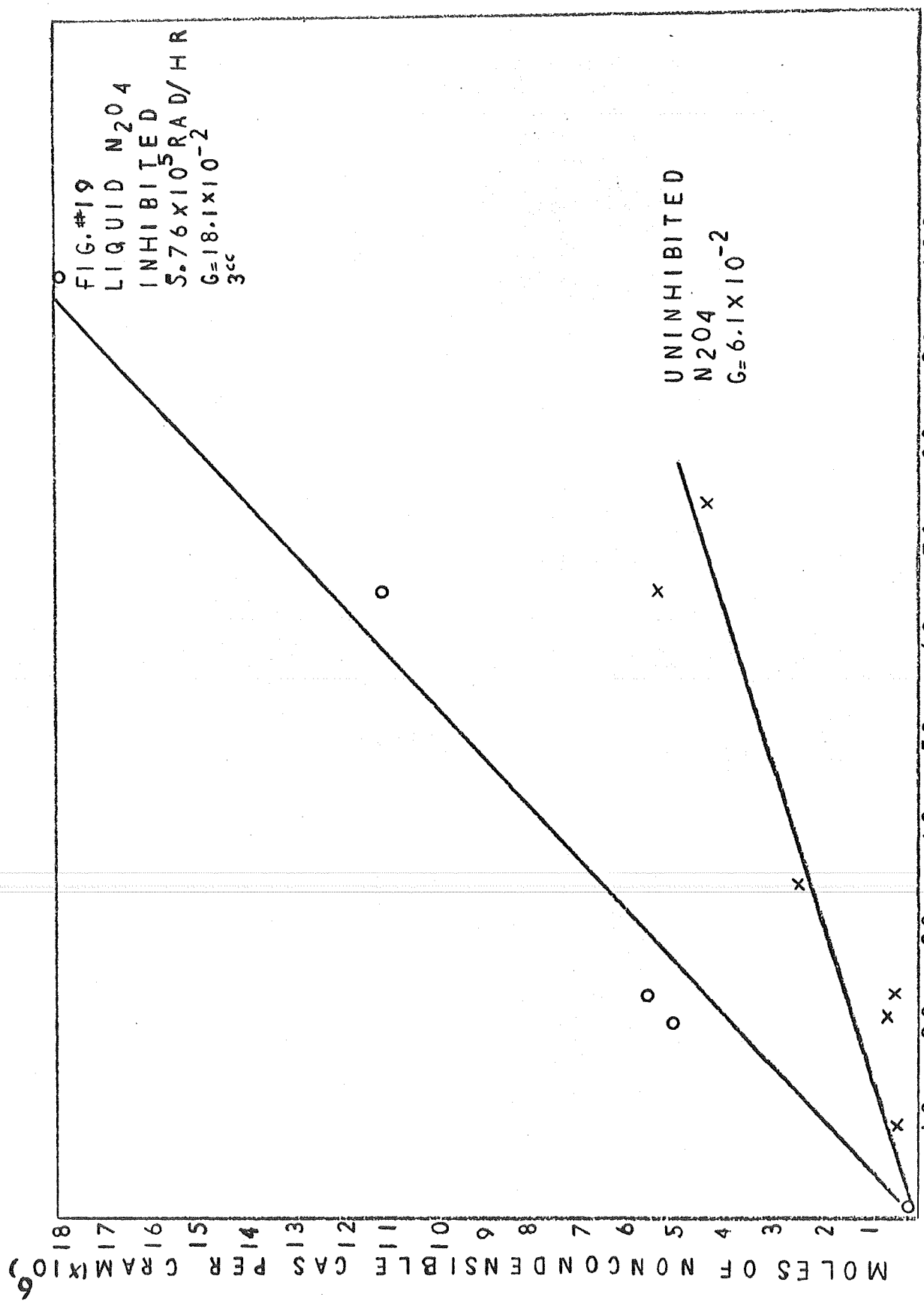
FIG. #19
LIQUID N_2O_4
INHIBITED
5.76×10^5 RAD/HR
$G = 18.1 \times 10^{-2}$
3cc
UNINHIBITED
N_2O_4
$G = 6.1 \times 10^{-2}$
MOLES OF NONCONDENSIBLE GAS PER GRAM ($\times 10^6$)
DOSE, MEGARAD
1
2
3
4
5
6
7
8
9
10
11
12
13
14
15
16
17
18
10
20
30
40
50
60
70
80
90
100

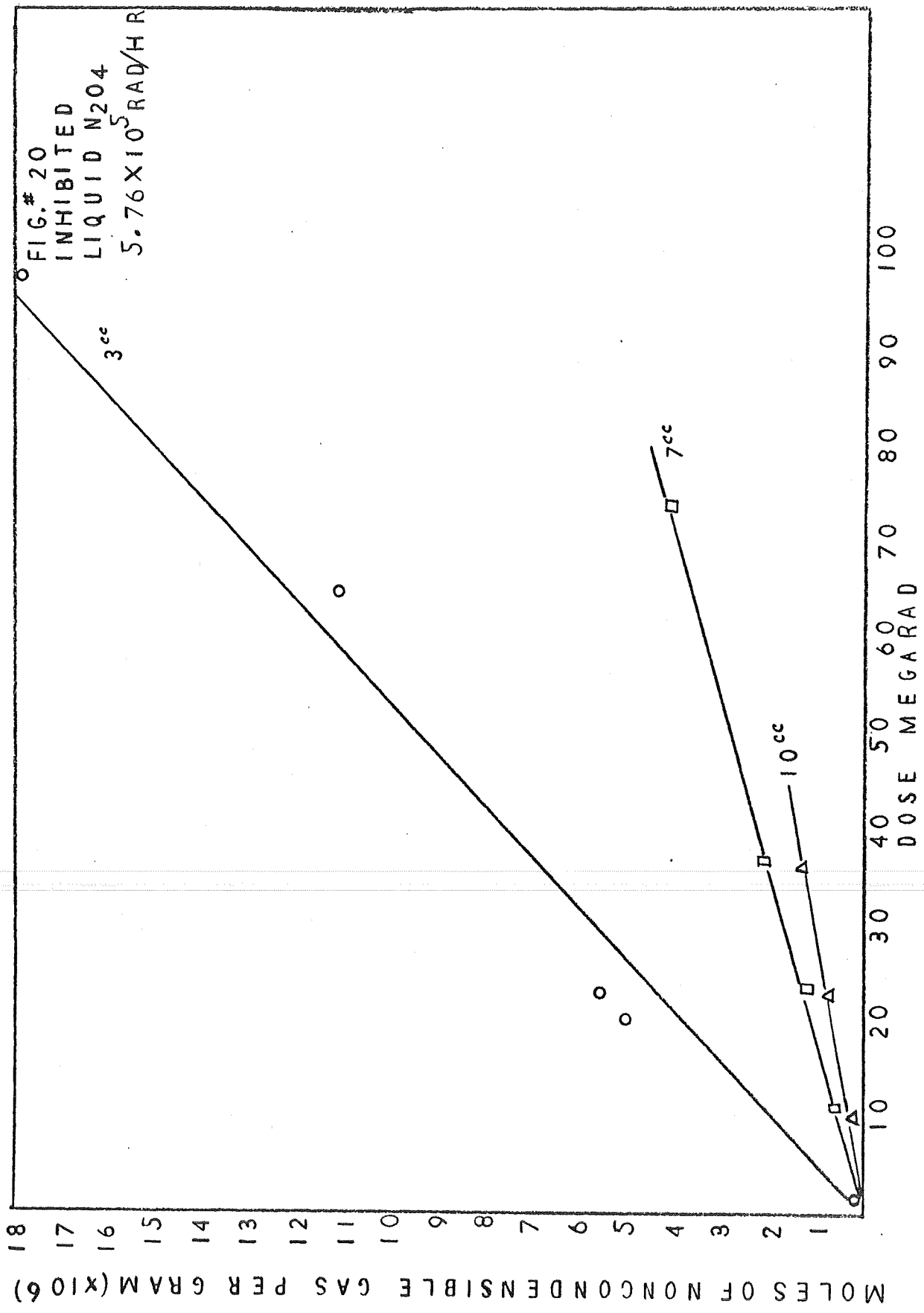
FIG.# 20
INHIBITED
LIQUID N_2O_4
5.76×10^5 RAD/HR
3 cc
7 cc
10 cc
MOLES OF NONCONDENSIBLE GAS PER GRAM (x10⁶)
DOSE MEGARAD
1
2
3
4
5
6
7
8
9
10
11
12
13
14
15
16
17
18
10
20
30
40
50
60
70
80
90
100

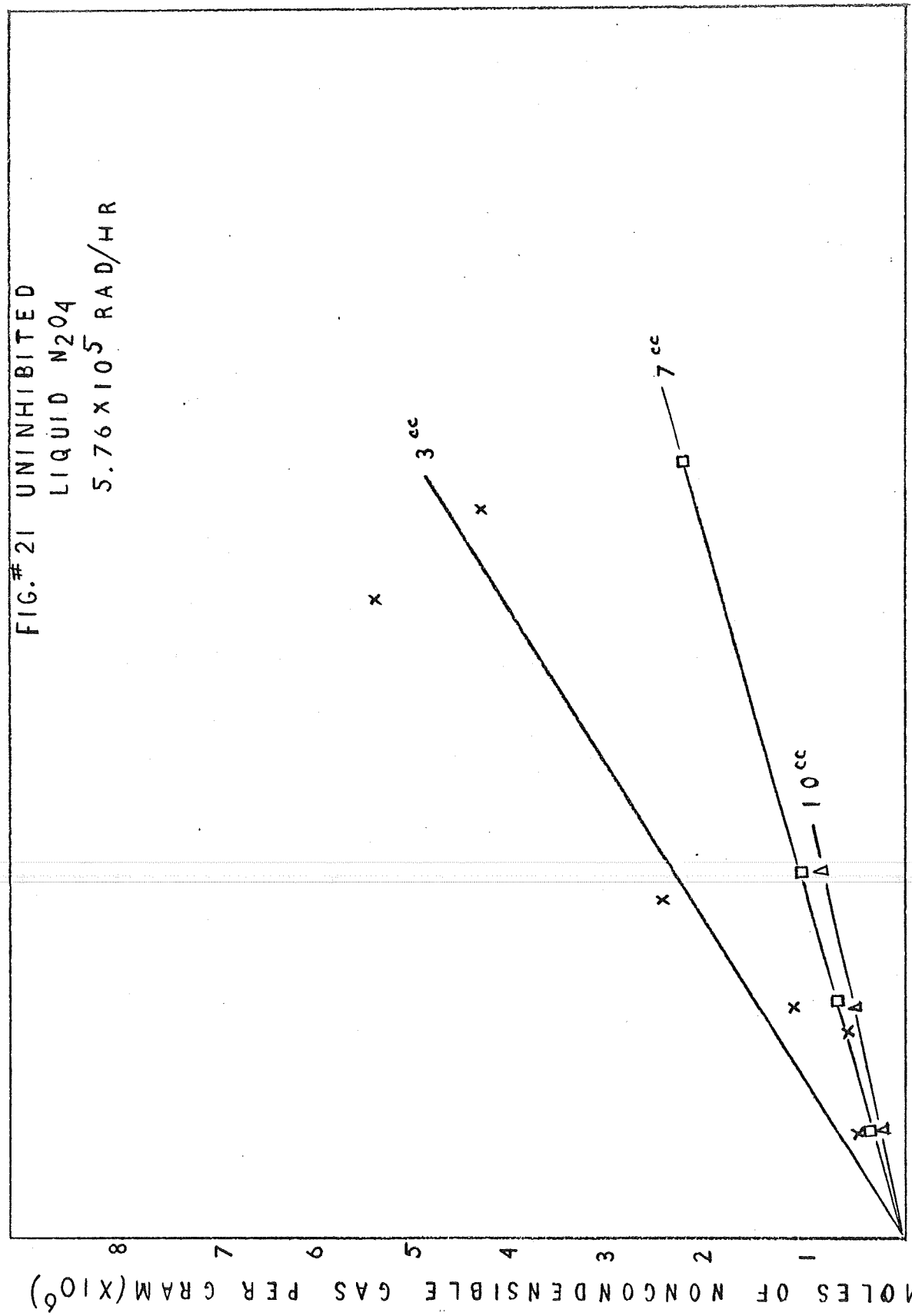
FIG. #21 UNINHIBITED
LIQUID N_2O_4
5.76×10^5 RAD/HR
3 cc
7 cc
10 cc
MOLES OF NONCONDENSIBLE GAS PER GRAM ($\times 10^6$)
DOSE MEGARAD
1
2
3
4
5
6
7
8
10
20
30
40
50
60
70
80
90
100

FIG# 22 LIQUID N_2O_4 AT~ 5.6×10^3 RAD/HR
Δ-INHIBITED
o-UNINHIBITED
MOLES OF GAS FORMED PER GRAM ($\times 10^6$)
1
2
3
4
5
6
7
5
10
15
20
25
30
35
40
45
50
DOSE MEGARAD

these numbers are only significant for the particular dose rate used, of course, but the observed differences between samples again suggests an interaction between the walls and nitrogen tetroxide vapor. It was also noted that the rate of the nonradiation decomposition, as indicated by buildup of gaseous products, was greater immediately after filling than at later times.

In several experiments all of the gases were examined rather than just the noncondensible species. The major component, excepting the N_2O_4, was NO in both the irradiated and nonirradiated cases and its rate of formation appeared about the same in both cases at the dose rate used, $5.7_6 \times 10^5$ rad/hr. Nitric oxide is an expected radiation decomposition product and a reasonable product of an oxidation reaction of NO_2 with the walls of the vessel.

It will be noted that the relative rates of radiation and nonradiation reactions is a direct function of the dose rate. At dose rates lower than those used in these experiments the effect of the radiation could be a small fraction of the overall reaction at least when storage vessels were not full of liquid.

The only significant noncondensible gas found on mass spectrometric analysis was nitrogen. The G-value for noncondensible gas formation then is the G-value for N_2 formation. For the uninhibited form $G(N_2) = 6.1 \times 10^{-2}$ molecules/100 ev which can be compared to the results reported by Castorina[10] of 5.2×10^{-2}. As seen in Figure 19, the G-value for the inhibited form is higher, being $G(N_2) = 18.1 \times 10^{-2}$ for the 3-cc samples. A summary of the G-values for noncondensible products at the various loadings is given below.

	N_2O_4 Inhibited	N_2O_4 Uninhibited
3 cc	18.1×10^{-2}	6.1×10^{-2}
7 cc	5.4×10^{-2}	2.8×10^{-2}
10 cc	3.6×10^{-2}	2.2×10^{-2}

The only other product found in addition to NO and N_2 was nitrous oxide (N_2O) which is formed at a rate slightly greater than that of nitrogen in the case of the uninhibited nitrogen tetroxide and slightly less in the case of the inhibited form. This again is consistent with the results of Castorina, who reported the formation of N_2O to be about half of that of N_2.

The lack of oxygen among the products is probably due to the NO formed, even in the absence of radiation. Any oxygen formed by decomposition of NO_2 by irradiation would react rapidly with NO to reform NO_2 or react with the wall which could act as a sink for the oxygen.

In general, the differences between the short-term and long-term experiments do not seem to be very large as can be seen from inspection of Figure 22. This indicates that the radiation decomposition in these cases is probably not strongly dependent on dose rate and the extent of decomposition will always be directly proportional to the radiation energy absorbed by the propellant material. The G-value corresponding to the line in the figure is 21×10^{-2} for a 3-cc sample compared to 18×10^{-2} for a 3-cc sample of the

inhibited N_2O_4 at high dose rate. The G-value for the uninhibited material at the low dose rate is somewhat higher, however, than the corresponding high dose rate case. Such differences as are seen may occur because thermal decomposition becomes a much larger factor at the lower dose rates. Although unirradiated "control" experiments have been carried out for each material, uncertainty from this source becomes more significant in the low dose rate cases.

The apparent rate of the nonradiation induced gas product formation decreases with increasing exposure time. On the other hand, the radiation induced decomposition occurs at an essentially constant rate proportional to the dose rate. At the dose rate of these experiments, approximately 5.6×10^3 rad/hr, the thermal reaction predominated during the first 6 weeks of exposure. After that the rate of the thermal decomposition had fallen to the point where the radiation induced decomposition becomes the dominant factor in the buildup of noncondensible gases. With continued irradiation, the buildup of gaseous products per unit absorbed dose is about the same as observed in the high dose rate case, the inhibited N_2O_4 shows a somewhat higher rate of radiation decomposition than the uninhibited N_2O_4. Because decomposition is slow, the pressure buildup was only a few torr per month and the thermal contribution during the first couple of months was comparatively large. A small error in this correction could possibly account for the curve, as shown in Figure 22, not going through the origin as expected.

Summary of Radiation Effects Data

The most striking result is the obviously much larger sensitivity to radiation induced decomposition of the fuels, as a group, compared to the oxidizers. Although molecular oxidizers are more susceptible than elemental ones, e.g., FLOX or liquid oxygen, they are still much more stable in a radiation field than the fuels examined in this program. This has obvious implications in regard to the positioning of fuel and oxidizer storage containers with respect to nuclear power sources and any shielding incorporated in the system. Although there are some differences among the materials studied with regard to container material and dose rate, as discussed in the previous sections, a rough comparison among these materials is shown in Figure 23. Although such a comparison cannot be exact, it is nonetheless instructive.

Using data on isotope sources previously reported (Contract NAS7-577), off-gas volumes formed in various propellants by plutonium, curium, and strontium heat sources are estimated in the following tabulation. For purposes of the estimates, the sources are estimated to be 200,000 watt (th) at 1 foot for $^{238}PuO_2$ and $^{244}Cm_2O_3$, which would be equivalent to 10 kw(e) at 5 percent conversion. The corresponding estimated dose is 1.3×10^5 rad, $^{238}PuO_2$ and 1.1×10^6 rad, $^{244}Cm_2O_3$. A 2000-watt (th) (100 w electrical) $^{90}SrTiO_3$ source at 1 meter is assumed to give a dose of about 3×10^7 rad.

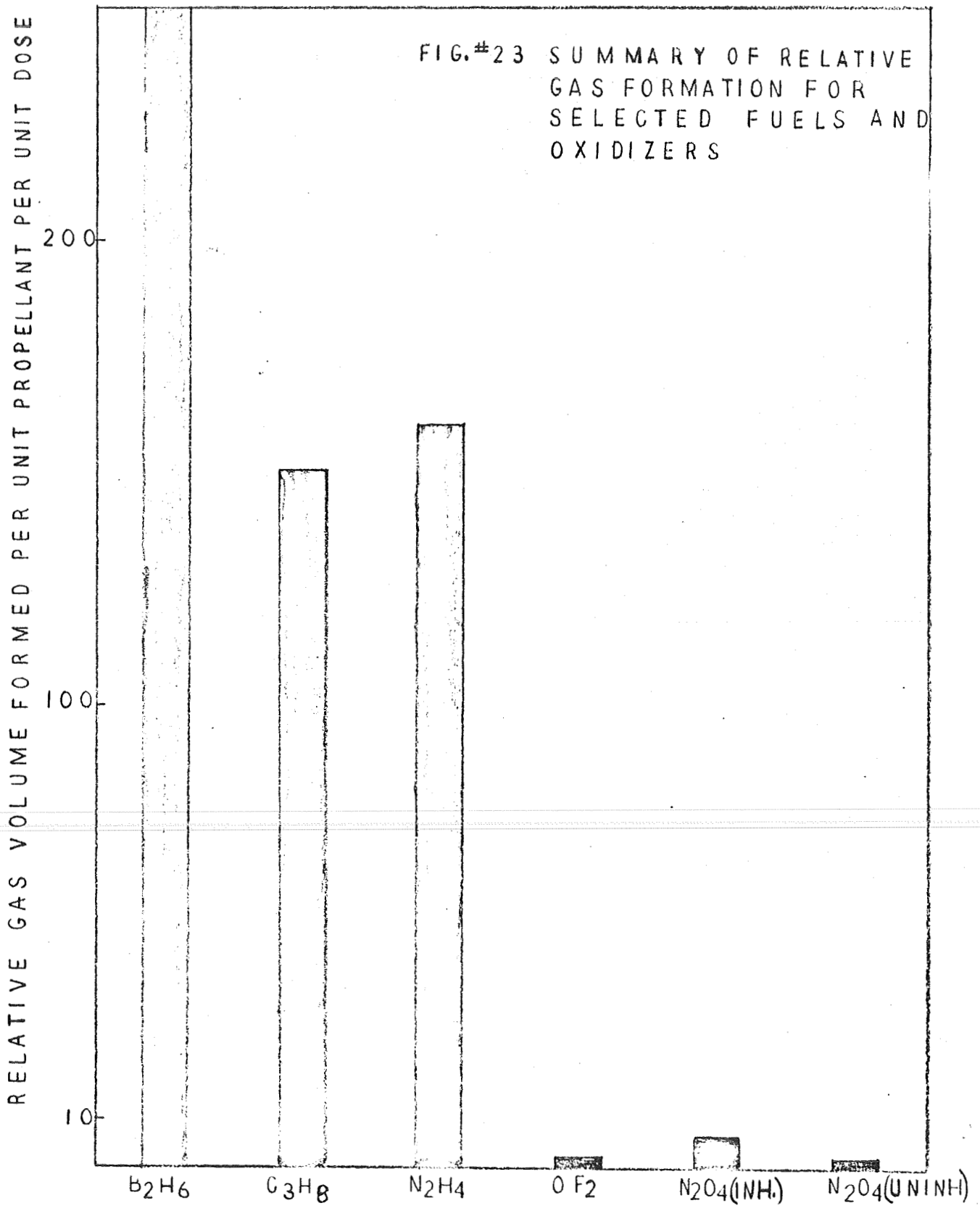

FIG.#23 SUMMARY OF RELATIVE GAS FORMATION FOR SELECTED FUELS AND OXIDIZERS

Propellant	Estimated Volume, ml, of Off-Gas Per Gram of Propellant Per Year		
	$^{238}PuO_2$	$^{244}Cm_2O_3$	$^{90}SrTiO_3$
B_2H_6	0.03	0.2	6
C_3H_8	0.02	0.1	5
N_2H_4	0.02	0.1	5
FLOX	0	0	0
OF_2	0.0003	0.0002	0.06
N_2O_4 (uninhibited)	0.0003	0.0002	0.06
N_2O_4 (inhibited)	0.0006	0.0004	0.1

The radiation doses used in the above estimates assume no self-shielding or external shielding. Since self-shielding will be significant in all of these sources at the power levels assumed, the estimates can be treated as maxima. It appears that the α-sources would present no large problems with these propellant materials over periods of several years. However, the ^{90}Sr β-sources might present some pressure buildup problems, at least in the case of fuels. From the experiments completed to date, it appears that the pressure would continue to build up over the propellant linearly with time over mission times of 1 to 10 years. The rate per unit time will depend on the size, configuration, and shielding of the radioisotope source. If the source decays significantly during the mission, a corresponding decrease in the rate of pressure buildup would be expected. That is, total noncondensable gas remains proportional to total dose. The accumulation of gas can be a significant engineering problem even though the amount of liquid decomposed by the radiation is relatively small and, of itself, probably not significant. Determining how best to accommodate those gaseous products which are formed could require a major technological effort.

Because there are indications of some interactions resulting from surface effects with particular propellant materials and specific container materials as well as some unexplained differences at low dose rates, additional research probably will be needed on specific propellant systems as these become better defined for given missions. This appears to be particularly true for the hydrazine and diborane fuels and the nitrogen tetroxide oxidizer. Interactions with container materials may well lead to pressure buildup of a similar nature to that from radiation. For long missions where the radiation dose rate might be expected to be minimum, surface interactions with the container might well be the major source of gaseous products. Shielding of the radiation source would then not accomplish the desired reduction in gaseous product accumulation. Further, the rate of such nonradiation decomposition would be expected to be a much stronger function of temperature than is the radiation induced reaction. The influence of this factor might only become apparent at low dose rates. Thus, further research should be directed at the elucidation of these factors. Only a more thorough understanding of the mechanisms, both radiation and nonradiation, and their interaction will permit more reliable predictions of gas buildup to long periods of time.

REFERENCES

(1) Engle, W. W., Jr., "A User's Manual for ANISN - A One-Dimensional Discrete Ordinates Code With Anisotropic Scattering", K-1693 (1967).

(2) Cornelius, G. K., et al., Aerojet-General Corporation, AFRPL-TR-64-146, Vol 1, October, 1964.

(3) Faust, J. P., Gould, J. R., and Kalman, M. H., U.S. Patent 3,001,920, September 26, 1961.

(4) Gillis, H. A., J. Phys. Chem., 71, 1089 (1967).

(5) Bone and Firestone, J. Phys. Chem., 69, 3652 (1965).

(6) Sieck and Johnson, J. Phys. Chem., 67, 2281 (1963).

(7) Lucien, H. W., and Pinns, M. L., "The X-Irradiation of Hydrazine and 1, 1-Dimethylhydrazine", Lewis Research Center, Cleveland, Ohio, NASA-TN-D-2452, August, 1964.

(8) Shelberg, W. E., "The Radiolytic Decomposition of Hydrazine RP-1 and Hydyne Rocket Fuels", U.S. Naval Radiological Defense Laboratory, San Francisco, California, USNRDL-TR-1002, March 6, 1966.

(9) Plank, H. F., "RIFT Radiation Effects Program Irradiation No. 9 Monomethyl Hydrazine", Lockheed Missiles and Space Company, Sunnyvale, California, NSP-64-10, February 15, 1964.

(10) Castorina, T. C., Picatinny Arsenal, Technical Report 3072, May, 1963.

APPENDIX A

DEFINITION OF COMMONLY USED TERMS (NOMENCLATURE)

APPENDIX A

DEFINITION OF COMMONLY USED TERMS (NOMENCLATURE)

Split Shield. A shield configuration consisting of two separate shields, one between the radiation source and the propellant tanks and one between the propellant tanks and the instrument package.

Laminated Shield. A shield configuration consisting of multi-layered shield component(s).

Shield Segment. One of the shields in the split-shield configuration.

Primary Direct Shield. The shield segment between the radiation source and the propellant tanks.

Secondary Direct Shield. The shield segment between the propellant tanks and the instrument package.

Scattering Structure. Any structure which may reflect a portion of radiation incident upon it to the propellant tanks or instrument package.

Scatter Shield. A shield used for the purpose of reducing the radiation reaching a scattering structure.

APPENDIX B

TRANSMISSION MATRIX DERIVATION AND USE

APPENDIX B

TRANSMISSION MATRIX DERIVATION AND USE

A Laplace transformed transmitted flux function may be written:

$$F(S) = H(S) \cdot G(S) \quad ,$$

where

F(S) is the Laplace transform of the transmitted flux function,
G(S) is the Laplace transform of the incident flux function, and
H(S) is the Laplace transform of the transmission function.

Since it is not intended to determine the Laplace transformation of all source distribution which may occur, the simplest and most useful source function, a delta function in energy denoted $\delta(E)$, is chosen. The Laplace transform of the delta function is unity and, therefore, simplifies the analysis considerably since any source spectrum may be described as a continuum of discrete energy sources. Thus:

$$F(S) = H(S) \cdot 1$$

or $$F(S) = H(S).$$

This implies that the inverse Laplace transforms of F(S) and H(S) are identical. Therefore, if discrete excitation energy-group transmission data are available, it is possible to construct the transmission function for any arbitrary input spectrum by summing up the discrete excitation transmission functions.

The advantage of using the transmission functions is that the group-to-group transfer matrix which is made up of point values from the transmission function is totally described for a given slab thickness. Thus, iterative solutions are not needed and significantly less computation time is anticipated. For laminated or multilayered shield configurations, this technique eliminates the uncertainty in buildup factor determination in the case of gamma radiation and also eliminates the necessity for use of fictitious removal cross-section information in the case of neutron radiation.

The most important assumption inherent in the technique is that double reflections across material boundaries are insignificant* contributors to the final solution.

---

* Ph.D. thesis, J. L. Ridihalgh, Iowa State University, 1968.

APPENDIX C

LISTING OF THE OPTIMIZATION COMPUTER PROGRAM FOR THE PRIMARY DIRECT LAMINATED SHIELD

APPENDIX C

LISTING OF THE OPTIMIZATION COMPUTER PROGRAM FOR THE PRIMARY DIRECT LAMINATED SHIELD

A listing of the optimization computer program for the primary direct laminated shield appears in this appendix along with sample-problem input data and output. The computer program consists of seven routines. They are:

(1) The main program which performs the iteration-control functions necessary to properly optimize the shield system

(2) Subroutine Geom which sets up the geometry information necessary for the program operations

(3) Subroutine WATE which determines the weight of any shield system designed by the program

(4) Subroutine Transf which reads radiation transmission factor information for the source and shield components

(5) Subroutine Flux which computes the radiation transmitted through the shield to the propellant tank

(6) Subroutine Source which computes the source radiation arriving at the front face of the shield

(7) Subroutine Intrp which is used by Subroutines Source and Flux to perform the interpolations and/or extrapolations on the transmission factor data.

Sample Problem

The sample problem is a two-group two-laminate shield optimization problem. The transmission factors used are purely fictitious since the problem was set up only to demonstrate the program operations. The order of input data for this problem is:

(1) Diameter of source - 5 cm - DSRC

(2) Length of source - 10 cm - XLSRC

(3) Diameter of propellant tank - 30 cm - DTANK

(4) Separation distance between propellant tank and the radiation source - 100 cm - SEPAR

(5) Number of shield laminates - 2 - LAM

(6) First guess of laminate thicknesses - 5., 5. - X(I)

(7) Density of shield laminates - 2., 1. - RHØ(I)

(8) Number of energy groups - 2 - NØG

(9) Dose conversion factors - 1.E-4, 1.E-5 - FD(I)

(10) Limiting dose rate - 1. - DRLIM

(11) Source strengths/vol - 1.E+10, 0. - SRCF(I)

(12) Number of thicknesses for which the transmission factors are inputed - 4 - NTHK

(13) Thicknesses for the shield laminates for which the transmission factors apply -

First Laminate	Second Laminate
1 cm	1 cm
2	2
8	8
16	16

1, 1, 2, 2, 8, 8, 16, 16 - TKTLM(I,J)

where I = Laminate Numbers 1 and 2

J = Thickness Numbers 1 to 4

(14) Transmission factors for the source material -

First Thickness	
0.9	0.
0.1	0.95

Second Thickness	
0.8	0.
0.2	0.89

Third Thickness	
0.6	0.
0.4	0.8

Fourth Thickness	
0.3	0.
0.7	0.6

where the matrix is $\begin{vmatrix} 11 & 12 \\ 21 & 22 \end{vmatrix}$

Position 11 - Group 1 transmission for Group 1 incidence

Position 12 - Group 1 transmission for Group 2 incidence

Position 21 - Group 2 transmission for Group 1 incidence

Position 22 - Group 2 transmission for Group 2 incidence

- TSRC (I,J,K)

where I = receiver group number

J = incidence group number

K = thickness number

(15) Thicknesses for the source for which the transmission factors apply - 1, 2, 4, 8 - TKSR(I)

where I = thickness number

(16) Transmission factors for the shield laminate materials

Material for First Laminate		Material for Second Laminate	
First Thickness			
0.5	0	0.9	0
0.49	0.99	0.1	0.5
Second Thickness			
0.25	0	0.8	0
0.72	0.98	0.19	0.25
Third Thickness			
0.02	0	0.5	0
0.9	0.9	0.4	0.02
Fourth Thickness			
0.0005	0	0.25	0
0.8	0.8	0.2	0.0005

The actual input and resultant program output are listed below.

Input

```
$DATA
 5.,10.,30.,100.,2,5.,5.,2.,1.,2,.0001,1.E-5,1.,1.E+10,
  0.,4,1.,1.,2.,2.,3.,3.,16.,16.,.9,0.,.1,.95,.8,0.,.2,.89,
  .6,0.,.4,.8,.3,0.,.7,.6,1.,2.,4.,8.,.5,0.,.49,.99,.9,0.,
  .1,.5,.25,0.,.72,.98,.8,0.,.19,.25,.02,0.,.9,.9,.5,0.,
  .4,.02,.0005,0.,.8,.8,.25,0.,.2,.0005
```

Output

```
ITERATION MONITOR
  15.1661          15.1661          1064.5226
  14.1006          17.2341          1145.7562
  15.1303          15.1303          1066.146
  16.5302          13.2241          1025.9523
  20.5709          12.7539          1233.671
LAMINATE THICKNESSES                WEIGHT
  16.4003          13.1202          1025.9523
```

Program Listing

```
10  COMMON RHO(2)
20  COMMON X(2),FD(2),SRCF(2),TLAM(2,2,2,4),TSRC(2,2,4),TKTLM(2,4),
30 +TKSRC(4),RATIO(2),SLOP,RMIN,DSRC,DTANK,LAM,XLSRC,SEPAR,WEIGHT,
40 +NOG
50  IJ=1
60  CALL GEOM
65  WEIGHT=100000.
80  READ,NOG,(FD(I),I=1,NOG),DRLIM
90  READ,(SRCF(I),I=1,NOG)
110  CALL TRANSF(NTHK)
111  PRINT,"      ITERATION MONITOR"
130  12  CALL FLUX(NTHK,DOSE)
140  IF(DRLIM-DOSE)9
150  IF(DRLIM-.1*DRLIM-DOSE)10
151  IF(DOSE-DRLIM)20
155  YY=0.
160  DO 11 I=1,LAM
165  YY=YY+X(I)
170  11  X(I)=X(I)*.9
175  IF(YY-.1)18
190  GO TO 12
191  20  DO 21 I=1,LAM
192  21  X(I)=X(I)*.98
193  GO TO 12
200  9  DO 13 I=1,LAM
210  13  X(I)=X(I)*1.12
220  GO TO 12
230  10  XX=0.
240  DO 14 I=1,LAM
250  14  XX=XX+X(I)
260  DO 15 I=1,LAM
270  15  RATIO(I)=X(I)/XX
280  CALL WATE(WT)
290  IF(2-IJ)18
295  PRINT,(X(I),I=1,LAM),WT
300  IF(1.01*WEIGHT-WT)19
310  WEIGHT=WT
320  IF(1-IJ)17
330  IF(.99-RATIO(1))18
340  IJ=1
350  RATIO(1)=.9*RATIO(1)
360  RATIO(2)=1.-RATIO(1)
370  X(1)=RATIO(1)*XX
380  X(2)=XX-X(1)
390  IF(X(1)-.01*XX)18
400  GO TO 12
410  19  IF(IJ-2)17
420  GO TO 16
430  17  IJ=2
435  WEIGHT=WT
440  X(1)=RATIO(1)*XX/.9
450  X(2)=XX-X(1)
460  IF(X(2)-.01*XX)18
470  GO TO 12
480  16  X(1)=RATIO(1)*XX*.9
490  X(2)=XX-X(1)
500  IJ=3
510  GO TO 12
520  18  PRINT,"      LAMINATE THICKNESSES              WEIGHT"
530  PRINT,(X(I),I=1,LAM),WEIGHT
```

```
      SUBROUTINE GEOM
      COMMON RHO(2)
      COMMON X(2),FD(2),SRCF(2),TLAM(2,2,2,4)TSRC(2,2,4),TKTLM(2,4),
     +TKSRC(4),RATIO(2),SLOP,RMIN,DSRC,DTANK,LAM,XLSRC,SEPAR,WEIGHT,
     +NOG
      READ,DSRC,XLSRC,DTANK,SEPAR,LAM,(X(I),I=1,LAM)
      READ,(RHO(I),I=1,LAM)
      IF(DSRC-DTANK)2
      SLOP=.5*(DTANK-DSRC)/(SEPAR+.5*DTANK)
      RMIN=.5*DSRC+SLOP*SEPAR
      GO TO 3
    2 SLOP=.5*(DTANK-DSRC)/(SEPAR+.5*DTANK+XLSRC)
      RMIN=.5*DSRC+SLOP*XLSRC
    3 CONTINUE
      CALL WATE(WT)
      WEIGHT=WT
      RETURN
      SUBROUTINE WATE(WT)
      DIMENSION A(2),VOL(2)
      COMMON RHO(2)
      COMMON X(2),FD(2),SRCF(2),TLAM(2,2,2,4),TSRC(2,2,4),TKTLM(2,4),
     +TKSRC(4),RATIO(2),SLOP,RMIN,DSRC,DTANK,LAM,XLSRC,SEPAR,WEIGHT,
     +NOG
      WT=0.
      RMIN1=RMIN
      DO 4 K=1,LAM
      IF(K-2)5
      A(K)=A(K-1)+SLOP*X(K)
      GO TO 4
    5 IF(DSRC-DTANK)6
      DO 7 I=1,LAM
    7 RMIN1=RMIN-X(I)*SLOP
    6 A(1)=RMIN1
    4 CONTINUE
      DO 8 K=1,LAM
      VOL(K)=(A(K)**2)*X(K)+SLOP*(A(K)*X(K)**2+SLOP/3.*X(K)**3)
    8 WT=VOL(K)*RHO(K)+WT
      RETURN
      SUBROUTINE TRANSF(NTHK)
      COMMON RHO(2)
      COMMON X(2),FD(2),SRCF(2),TLAM(2,2,2,4),TSRC(2,2,4),TKTLM(2,4),
     +TKSRC(4),RATIO(2),SLOP,RMIN,DSRC,DTANK,LAM,XLSRC,SEPAR,WEIGHT,
     +NOG
      READ,NTHK,((TKTLM(I,J),I=1,LAM),J=1,NTHK)
      READ,(((TSRC(I,J,K),I=1,NOG),J=1,NOG),K=1,NTHK)
      READ,(TKSRC(I),I=1,NTHK)
      READ,((((TLAM(I,J,K,L),I=1,NOG),J=1,NOG),K=1,LAM),L=1,NTHK)
      RETURN
```

```
      SUBROUTINE FLUX(NTHK,DOSE)
      COMMON RHO(2)
      COMMON X(2),FD(2),SRCF(2),TLAM(2,2,2,4),TSRC(2,2,4),TKTLM(2,4),
     +TKSRC(4),RATIO(2),SLOP,RMIN,DSRC,DTANK,LAM,XLSRC,SEPAR,WEIGHT,
     +NOG
      DIMENSION FLU(2),FLUX(2)
      DO 3 I=1,NOG
      FLUX(I)=0.
    3 FLU(I)=0.
      GO TO 8
    5 DO 2 K=1,LAM
      DO 1 I=1,NOG
      DO 1 J=I,NOG
      CALL INTRP(I,J,K,X(K),TL,NTHK)
      FLUX(J)=FLU(I)*TL+FLUX(J)
    1 CONTINUE
      DO 2 I=1,NOG
      FLU(I)=FLUX(I)
      FLUX(I)=0.
    2 CONTINUE
      DOSE=0.
      DO 6 I=1,NOG
    6 DOSE=DOSE+FD(I)*FLU(I)
      DOSE=DOSE/(12.566*SEPAR**2)
      RETURN
    8 CALL SOURCE(FLU,NTHK)
      GO TO 5
      RETURN
      SUBROUTINE SOURCE(FLU,NTHK)
      COMMON RHO(2)
      COMMON X(2),FD(2),SRCF(2),TLAM(2,2,2,4),TSRC(2,2,4),
     +TKTLM(2,4),TKSRC(4),RATIO(2),SLOP,RMIN,DSRC,DTANK,LAM,XLSRC,
     +SEPAR,WEIGHT,NOG
      DIMENSION FLU(2),FLUX(2),FRU(2)
      DO 1 I=1,NOG
    1 FRU(I)=0.
      DO 4 M=1,10
      XSRC=XLSRC/10.*(M-1)+XLSRC/20.
      DO 3 K=1,NOG
    3 FLU(K)=(SRCF(K)*.785*DSRC**2)*XLSRC/10.
      DO 2 I=1,NOG
      DO 2 J=I,NOG
      CALL INTRP(I,J,0,XSRC,TS,NTHK)
      FLUX(J)=FLU(I)*TS+FLUX(J)
    2 CONTINUE
      DO 4 I=1,NOG
      FRU(I)=FLUX(I)+FRU(I)
    4 FLUX(I)=0.
      DO 7 I=1,NOG
    7 FLU(I)=FRU(I)
      RETURN
```

```
1150  SUBROUTINE INTRP(I,J,K,X1,T,N)
1155  COMMON RHO(2)
1160  COMMON X(2),FD(2),SRCF(2),TLAM(2,2,2,4),TSRC(2,2,4),TKTLM(2,4),
1165  +TKSRC(4),RATIO(2),SLOP,RMIN,DSRC,DTANK,LAM,XLSRC,SEPAR,
1170  +WEIGHT,NOG
1175  IF(K-1)1
1180  DO 2 II=1,N
1185  2  IF(X1-TKTLM(K,II))3
1190  Z=X1-TKTLM(K,N)
1195  H=TKTLM(K,N)-TKTLM(K,N-1)
2000  R=TLAM(I,J,K,N)-TLAM(I,J,K,N-1)
2005  T=TLAM(I,J,K,N)+R/H*Z
2006  IF(T)11
2007  IF(1.-T)12
2010  RETURN
2011  11  T=0.;  RETURN
2012  12  T=1.;  RETURN
2015  3  IF(II-2)4
2020  Z=(X1-TKTLM(K,II-1))/(TKTLM(K,II)-TKTLM(K,II-1))
2025  H=TLAM(I,J,K,II)-TLAM(I,J,K,II-1)
2030  T=TLAM(I,J,K,II-1)+H*Z
2035  RETURN
2040  4  IF(J-I-1)9
2050  T=X1/TKTLM(K,1)*TLAM(I,J,K,1)
2055  RETURN
2056  9  T=1.-X1/TKTLM(K,1)*(1.-TLAM(I,J,K,1))
2057  RETURN
2060  1  DO 5 II=1,NTHK
2065  5  IF(X1-TKSRC(II))6
2070  Z=X1-TKSRC(N)
2075  H=TKSRC(N)-TKSRC(N-1)
2080  R=TSRC(I,J,N)-TSRC(I,J,N-1)
2085  T=TSRC(I,J,N)+R/H*Z
2086  IF(T)11
2087  IF(1.-T)12
2090  RETURN
2095  6  IF(II-2)7
2100  Z=(X1-TKSRC(II-1))/(TKSRC(II)-TKSRC(II-1))
2105  H=TSRC(I,J,II)-TSRC(I,J,II-1)
2110  T=TSRC(I,J,II-1)+H*Z
2115  RETURN
2120  7  IF(J-I-1)13
2130  T=X1/TKSRC(1)*TSRC(I,J,1)
2135  RETURN
2136  13  T=1.-X1/TKSRC(1)*(1.-TSRC(I,J,1))
2137  RETURN
2140  END
2200 $USE DAT1
```

REPORT IS TO BE SENT DIRECTLY TO THE -RECIPIENTS- MARKED WITH AN -X- UNDER THE COLUMN HEADED -DESIGNEE- (FIRST SECTION ONLY). IN FOLLOWING SECTIONS, THE REPORT SHOULD BE SENT TO THE TECHNICAL LIBRARIAN OF THE -RECIPIENT- WITH A CARBON COPY OF THE LETTER OF TRANSMITTAL TO THE ATTENTION OF THE PERSON NAMED UNDER THE COLUMN DESIGNEE. THE LETTER OF TRANSMITTAL SHOULD CONTAIN THE CONTRACT NUMBER AND COMPLETE TITLE OF THE FINAL REPORT.

THE DISTRIBUTION LIST SHOULD BE INCLUDED IN THE FINAL REPORT AS AN APPENDIX.

DISTRIBUTION LIST FOR FINAL REPORT

CONTRACT NAS7-722

COPIES	RECIPIENT	DESIGNEE
	NASA HEADQUARTERS WASHINGTON, D.C. 20546	
1	CONTRACTING OFFICER	(X)
1	PATENT OFFICE	(X)
	NASA LEWIS RESEARCH CENTER 21000 BROOKPARK RD. CLEVELAND, OHIO 44135	
1	OFFICE OF TECHNICAL INFORMATION	(X)
	NASA MANNED SPACECRAFT CENTER HOUSTON, TEXAS 77001	
1	OFFICE OF TECHNICAL INFORMATION	(X)
	NASA MARSHALL SPACE FLIGHT CENTER HUNTSVILLE, ALABAMA 35812	
2	OFFICE OF TECHNICAL INFORMATION, MS-IP	(X)
1	TECHNICAL LIBRARY	(X)
1	DALE BURROWS, S & E-ASTN-PJ	(X)
	NASA PASADENA OFFICE 4800 OAK GROVE DRIVE PASADENA, CALIFORNIA 91103	
1	PATENTS AND CONTRACTS MANAGEMENT	(X)
	JET PROPULSION LABORATORY 4800 OAK GROVE DR. PASADENA , CALIF. 91103	
2	ORVILLE F. KELLER	(X)
3	CHIEF, LIQUID PROPULSION TECHNOLOGY RPL NASA HEADQUARTERS WASHINGTON, D.C., 20546	(X)
1	DIRECTOR, TECHNOLOGY UTILIZATION DIVISION OFFICE OF TECHNOLOGY UTILIZATION NASA HEADQUARTERS	(X)

	WASHINGTON, D.C. 20546	
25	NASA SCIENTIFIC AND TECHNICAL INFORMATION FACILITY P.O. BOX 33 COLLEGE PARK, MARYLAND 20740	(X)
1	DIRECTOR , LAUNCH VEHICLES AND PROPULSION , SV OFFICE OF SPACE SCIENCE AND APPLICATIONS NASA HEADQUARTERS WASHINGTON , D. C. 20546	(X)
1	DIRECTOR, ADVANCED MANNED MISSIONS, MT OFFICE OF MANNED SPACE FLIGHT NASA HEADQUARTERS WASHINGTON , D. C. 20546	(X)
1	MISSION ANALYSIS DIVISION NASA AMES RESEARCH CENTER MOFFETT FIELD, CALIFORNIA 24035	(X)

NASA FIELD CENTERS

2	AMES RESEARCH CENTER MOFFETT FIELD, CALIFORNIA 94035	HANS M. MARK
1	GODDARD SPACE FLIGHT CENTER GREENBELT, MARYLAND 20771	MERLAND L. MOSESON CODE 620
2	JET PROPULSION LABORATORY CALIFORNIA INSTITUTE OF TECHNOLOGY 4800 OAK GROVE DRIVE PASADENA, CALIFORNIA 91103	HENRY BURLAGE, JR PROPULSION DIV. 38
2	LANGLEY RESEARCH CENTER LANGLEY STATION HAMPTON, VIRGINIA 23365	ED CORTWRIGHT DIRECTOR
2	LEWIS RESEARCH CENTER 21000 BROOKPARK ROAD CLEVELAND, OHIO 44135	DR. ABE SILVERSTEIN DIRECTOR
2	MARSHALL SPACE FLIGHT CENTER HUNTSVILLE, ALABAMA 35812	HANS G. PAUL CODE R-P+VED
2	MANNED SPACECRAFT CENTER HOUSTON, TEXAS 77001	J.G. THIBODAUX, JR. CHIEF, PROP. + POWER DIV.
2	JOHN F. KENNEDY SPACE CENTER, NASA COCOA BEACH, FLORIDA 32931	DR. KURT H. DEBUS

GOVERNMENT INSTALLATIONS

1	AERONAUTICAL SYSTEMS DIVISION	D.L. SCHMIDT

	AIR FORCE SYSTEMS COMMAND WRIGHT-PATTERSON AIR FORCE BASE DAYTON, OHIO 45433	CODE ASRCNC-2
1	AIR FORCE MISSILE DEVELOPMENT CENTER HOLLOMAN AIR FORCE BASE NEW MEXICO 88330	MAJ. R.F. BRACKEN
1	AIR FORCE MISSILE TEST CENTER PATRICK AIR FORCE BASE, FLORIDA	L.J. ULLIAN
1	SPACE AND MISSILE SYSTEMS ORGANIZATION AIR FORCE UNIT POST OFFICE LOS ANGELES 45, CALIFORNIA 90045	COL. CLARK TECHNICAL DATA CENTER
1	ARNOLD ENGINEERING DEVELOPMENT CENTER ARNOLD AIR FORCE STATION TULLAHOMA, TENNESSEE 37388	DR. H.K. DOETSCH
1	BUREAU OF NAVAL WEAPONS DEPARTMENT OF THE NAVY WASHINGTON , D. C. 20546	J. KAY RTMS-41
1	DEFENSE DOCUMENTATION CENTER HEADQUARTERS CAMERON STATION, BUILDING 5 5010 DUKE STREET ALEXANDRIA, VIRGINIA 22314 ATTN- TISIA	
1	HEADQUARTERS, U.S. AIR FORCE WASHINGTON 25, D.C. 20546	COL.C.K. STAMBAUGH AFRST
1	PICATINNY ARSENAL DOVER, NEW JERSEY 07801	I. FORSTEN, CHIEF LIQUID PROPULSION LABORATORY,
2	AIR FORCE ROCKET PROPULSION LABORATORY RESEARCH AND TECHNOLOGY DIVISION AIR FORCE SYSTEMS COMMAND EDWARDS, CALIFORNIA 93523	RPRPD/MR. H. MAIN
1	U.S. ARMY MISSILE COMMAND REDSTONE ARSENAL ALABAMA 35809	MR. WALTER WHARTON
1	U.S. NAVAL ORDNANCE TEST STATION CHINA LAKE CALIFORNIA 93557	CODE 4562 CHIEF, MISSILE PROPULSION DIV.

CPIA

1	CHEMICAL PROPULSION INFORMATION AGENCY APPLIED PHYSICS LABORATORY 8621 GEORGIA AVENUE	TOM REDDY

SILVER SPRING, MARYLAND 20910

INDUSTRY CONTRACTORS

1	AEROJET-GENERAL CORPORATION P. O. BOX 296 AZUSA, CALIFORNIA 91703	W. L. ROGERS
1	AEROJET-GENERAL CORPORATION P. O. BOX 1947 TECHNICAL LIBRARY, BLDG 2015, DEPT. 2410 SACRAMENTO, CALIFORNIA 95809	R. STIFF
1	SPACE DIVISION AEROJET-GENERAL CORPORATION 9200 EAST FLAIR DR. EL MONTE, CALIFORNIA 91734	S. MACHLAWSKI
1	AEROSPACE CORPORATION 2400 EAST EL SEGUNDO BOULEVARD P. O. BOX 95085 LOS ANGELES, CALIFORNIA 90045	JOHN G. WILDER MS-2293
1	ASTROSYSTEMS INTERNATIONAL, INC. 1275 BLOOMFIELD AVENUE FAIRFIELD, NEW JERSY 07007	A. MENDENHALL
1	ATLANTIC RESEARCH CORPORATION EDSALL ROAD AND SHIRLEY HIGHWAY ALEXANDRIA, VIRGINIA 22314	DR. RAY FRIEDMAN
1	AVCO SYSTEMS DIVISION WILMINGTON, MASSACHUSETTS	HOWARD B. WINKLER
1	BEECH AIRCRAFT CORPORATION BOULDER DIVISION BOX 631 BOULDER , COLORADO	J. H. RODGERS
1	BELL AEROSYSTEMS COMPANY P.O. BOX 1 BUFFALO, NEW YORK 14240	W. M. SMITH
1	BELLCOMM 955 L-ENFANT PLAZA, S. W. WASHINGTON, D. C.	H. S. LONDON
1	BENDIX SYSTEMS DIVISION BENDIX CORPORATION 3300 PLYMOUTH ROAD ANN ARBOR, MICHIGAN 48105	JOHN M. BRUEGER
1	BOEING COMPANY P. O. BOX 3707 SEATTLE, WASHINGTON 98124	J. D. ALEXANDER

1	BOEING COMPANY 1625 K STREET, N. W. WASHINGTON, D. C. 20006	LIBRARY
1	BOEING COMPANY P. O. BOX 1680 HUNTSVILLE, ALABAMA 35801	TED SNOW
1	MISSILE DIVISION CHRYSLER CORPORATION P. O. BOX 2628 DETROIT, MICHIGAN 48231	MR. JOHN GATES
1	WRIGHT AERONAUTICAL DIVISION CURTISS-WRIGHT CORPORATION WOOD-RIDGE, NEW JERSEY 07075	G. KELLEY
1	RESEARCH CENTER FAIRCHILD HILLER CORPORATION GERMANTOWN, MARYLAND	RALPH HALL
1	REPUBLIC AVIATION CORPORATION FAIRCHILD HILLER CORPORATION FARMINGDALE, LONG ISLAND, NEW YORK	LIBRARY
1	GENERAL DYNAMICS, CONVAIR DIVISION LIBRARY + INFORMATION SERVICES (128-00) P. O. BOX 1128 LOS ANGELES, CALIF. 90005	FRANK DORE
1	MISSILE AND SPACE SYSTEMS CENTER GENERAL ELECTRIC COMPANY VALLEY FORCE SPACE TECHNOLOGY CENTER P.O. BOX 8555 PHILADELPHIA, PA.	F. MEZGER F. E. SCHULTZ
1	GRUMMAN AIRCRAFT ENGINEERING CORP. BETHPAGE, LONG ISLAND NEW YORK 11714	JOSEPH GAVIN
1	HONEYWELL, INC. AEROSPACE DIV. 2600 RIDGWAY RD MINNEAPOLIS, MINN.	MR. GORDON HARMS
1	HUGHES AIRCRAFT CO. AEROSPACE GROUP CENTINELA AND TEALE STREETS CULVER CITY, CALIF. 90230	E. H. MEIER V.P.AND DIV. MGR., RESEARCH + DEV. DIV.
1	WALTER KIDDE AND COMPANY, INC. AEROSPACE OPERATIONS 567 MAIN STREET BELLEVILLE, NEW JERSEY	R. J. HANVILLE DIR. OF RESEARCH ENGR.
1	LING-TEMCO-VOUGHT CORPORATION P. O. BOX 5907 DALLAS, TEXAS 75222	WARREN G. TRENT

1	ARTHUR D. LITTLE, INC. 20 ACORN PARK CAMBRIDGE, MASSACHUSETTS 02140	LIBRARY
1	LOCKHEED MISSILES AND SPACE CO. ATTN-TECHNICAL INFORMATION CENTER P.O. BOX 504 SUNNYVALE, CALIFORNIA 94088	J. GUILL
1	LOCKHEED PROPULSION COMPANY P. O. BOX 111 REDLANDS, CALIFORNIA 92374	H. L. THACKWELL
1	THE MARQUARDT CORPORATION 16555 SATICOY STREET VAN NUYS ,CALIF. 91409	HOWARD MC FARLAND
1	BALTIMORE DIVISION MARTIN MARIETTA CORPORATION BALTIMORE, MARYLAND 21203	MR. JOHN CALATHES (3214)
1	DENVER DIVISION MARTIN MARIETTA CORPORATION P. O. BOX 179 DENVER, COLORADO 80201	DR MORGANTHALER A. J. KULLAS
1	ORLANDO DIVISION MARTIN MARIETTA CORP. BOX 5837 ORLANDO, FLORIDA	J. FERM
1	ASTROPOWER LABORATORY MC DONNELL-DOUGLAS AIRCRAFT COMPANY 2121 PAULARINO NEWPORT BEACH, CALIFORNIA 92663	DR. GEORGE MOC DIRECTOR, RESEARCH
1	MCDONNEL-DOUGLAS AIRCRAFT CORP. P. O. BOX 516 MUNICIPAL AIRPORT ST. LOUIS, MISSOURI 63166	R. A. HERZMARK
1	MISSILE AND SPACE SYSTEMS DIVISION MC DONNELL-DOUGLAS AIRCRAFT COMPANY 3000 OCEAN PARK BOULEVARD SANTA MONICA, CALIF. 90406	MR. R. W. HALLET CHIEF ENGINEER ADV. SPACE TECH.
1	SPACE+INFORMATION SYSTEMS DIVISION NORTH AMERICAN ROCKWELL 12214 LAKEWOOD BOULEVARD DOWNEY, CALIFORNIA 90241	LIBRARY
1	ROCKETDYNE (LIBRARY 586-306) 6633 CANOGA AVENUE CANOGA PARK, CALIF. 91304	DR. R. J. THOMPSON S. F. IACOBELLIS

1	NORTHROP SPACE LABORATORIES 3401 WEST BROADWAY HAWTHORNE, CALIFORNIA 90250	DR. WILLIAM HOWARD
1	AERONUTRONIC DIVISION PHILCO CORPORATION FORD ROAD NEWPORT BEACH, CALIFORNIA 92663	D. A. GARRISON
1	ASTRO-ELECTRONICS DIVISION RADIO CORPORATION OF AMERICA PRINCETON, NEW JERSEY 08540	Y. BRILL
1	ROCKET RESEARCH CORPORATION 520 SOUTH PORTLAND STREET SEATTLE, WASHINGTON 98108	FOY MCCULLOUGH, JR.
1	SUNSTRAND AVIATION 2421 11TH STREET ROCKFORD, ILLINOIS 61101	R. W. REYNOLDS
1	STANFORD RESEARCH INSTITUTE 333 RAVENSWOOD AVENUE MENLO PARK, CALIFORNIA 94025	DR. GERALD MARKSMAN
1	TRW SYSTEMS GROUP TRW INCORPORATED ONE SPACE PARK REDONDO BEACH, CALIF. 90278	G. W. ELVERUM
1	TAPCO DIVISION TRW, INCORPORATED 23555 EUCLID AVENUE CLEVELAND, OHIO 44117	P. T. ANGELL
1	THIOKOL CHEMICAL CORPORATION HUNTSVILLE DIVISION HUNTSVILLE, ALABAMA 35807	JOHN GOODLOE
1	RESEARCH LABORATORIES UNITED AIRCRAFT CORP. 400 MAIN ST. EAST HARTFORD, CONN. 06108	ERLE MARTIN
1	HAMILTON STANDARD DIVISON UNITED AIRCRAFT CORP. WINDSOR LOCKS, CONN. 06096	MR. R. HATCH
1	UNITED TECHNOLOGY CENTER 587 METHILDA AVENUE P. O. BOX 358 SUNNYVALE, CALIFORNIA 94088	DR. DAVID ALTMAN
1	FLORIDA RESEARCH AND DEVELOPMENT PRATT AND WHITNEY AIRCRAFT UNITED AIRCRAFT CORPORATION P. O. BOX 2691 WEST PALM BEACH, FLORIDA 33402	R.J. COAR

1 VICKERS, INC.
BOX 302
TROY, MICHIGAN